



International Agreement Report

Implementation of Advanced Multigroup Nodal and Pin Power Reconstruction Methods into PARCS 3.1

Prepared by:

Joo-il Yoon, Han Gyu Joo, Seung Hoon Ahn

Anthony Calvo, NRC Project Manager

**Office of Nuclear Regulatory Research
U.S. Nuclear Regulatory Commission
Washington, DC 20555-0001**

Manuscript Completed: December 2010

Date Published: May 2012

Prepared as part of
The Agreement on Research Participation and Technical Exchange
Under the Thermal-Hydraulic Code Applications and Maintenance Program (CAMP)

**Published by
U.S. Nuclear Regulatory Commission**

**AVAILABILITY OF REFERENCE MATERIALS
IN NRC PUBLICATIONS**

NRC Reference Material

As of November 1999, you may electronically access NUREG-series publications and other NRC records at NRC's Public Electronic Reading Room at <http://www.nrc.gov/reading-rm.html>. Publicly released records include, to name a few, NUREG-series publications; *Federal Register* notices; applicant, licensee, and vendor documents and correspondence; NRC correspondence and internal memoranda; bulletins and information notices; inspection and investigative reports; licensee event reports; and Commission papers and their attachments.

NRC publications in the NUREG series, NRC regulations, and *Title 10, Energy*, in the Code of *Federal Regulations* may also be purchased from one of these two sources.

1. The Superintendent of Documents
U.S. Government Printing Office
Mail Stop SSOP
Washington, DC 20402-0001
Internet: bookstore.gpo.gov
Telephone: 202-512-1800
Fax: 202-512-2250
2. The National Technical Information Service
Springfield, VA 22161-0002
www.ntis.gov
1-800-553-6847 or, locally, 703-605-6000

A single copy of each NRC draft report for comment is available free, to the extent of supply, upon written request as follows:

Address: U.S. Nuclear Regulatory Commission
Office of Administration
Publications Branch
Washington, DC 20555-0001
E-mail: DISTRIBUTION.RESOURCE@NRC.GOV
Facsimile: 301-415-2289

Some publications in the NUREG series that are posted at NRC's Web site address <http://www.nrc.gov/reading-rm/doc-collections/nuregs> are updated periodically and may differ from the last printed version. Although references to material found on a Web site bear the date the material was accessed, the material available on the date cited may subsequently be removed from the site.

Non-NRC Reference Material

Documents available from public and special technical libraries include all open literature items, such as books, journal articles, and transactions, *Federal Register* notices, Federal and State legislation, and congressional reports. Such documents as theses, dissertations, foreign reports and translations, and non-NRC conference proceedings may be purchased from their sponsoring organization.

Copies of industry codes and standards used in a substantive manner in the NRC regulatory process are maintained at—

The NRC Technical Library
Two White Flint North
11545 Rockville Pike
Rockville, MD 20852-2738

These standards are available in the library for reference use by the public. Codes and standards are usually copyrighted and may be purchased from the originating organization or, if they are American National Standards, from—

American National Standards Institute
11 West 42nd Street
New York, NY 10036-8002
www.ansi.org
212-642-4900

Legally binding regulatory requirements are stated only in laws; NRC regulations; licenses, including technical specifications; or orders, not in NUREG-series publications. The views expressed in contractor-prepared publications in this series are not necessarily those of the NRC.

The NUREG series comprises (1) technical and administrative reports and books prepared by the staff (NUREG-XXXX) or agency contractors (NUREG/CR-XXXX), (2) proceedings of conferences (NUREG/CP-XXXX), (3) reports resulting from international agreements (NUREG/IA-XXXX), (4) brochures (NUREG/BR-XXXX), and (5) compilations of legal decisions and orders of the Commission and Atomic and Safety Licensing Boards and of Directors' decisions under Section 2.206 of NRC's regulations (NUREG-0750).

DISCLAIMER: This report was prepared under an international cooperative agreement for the exchange of technical information. Neither the U.S. Government nor any agency thereof, nor any employee, makes any warranty, expressed or implied, or assumes any legal liability or responsibility for any third party's use, or the results of such use, of any information, apparatus, product or process disclosed in this publication, or represents that its use by such third party would not infringe privately owned rights.



International Agreement Report

Implementation of Advanced Multigroup Nodal and Pin Power Reconstruction Methods into PARCS 3.1

Prepared by:

Joo-il Yoon, Han Gyu Joo, Seung Hoon Ahn

Anthony Calvo, NRC Project Manager

**Office of Nuclear Regulatory Research
U.S. Nuclear Regulatory Commission
Washington, DC 20555-0001**

Manuscript Completed: December 2010

Date Published: May 2012

Prepared as part of
The Agreement on Research Participation and Technical Exchange
Under the Thermal-Hydraulic Code Applications and Maintenance Program (CAMP)

**Published by
U.S. Nuclear Regulatory Commission**

ABSTRACT

The original multi-group solver of PARCS uses a nodal expansion method combined with one-node calculation scheme. But the neutronics solver was inefficient for application to the real-size reactor cores because of its slow performance. Moreover, the existing pin power reconstruction with the corner point balancing method does not support the multi-group structure. In order to improve the performance for multi-group problems, the semi-analytic nodal method and pin power reconstruction with the source expansion formulation have been incorporated into the PARCS code. The purpose of the nodal formulation is to solve the transverse-integrated one-dimensional neutron balance equation. Also, a two-level CMFD method in which the two-group CMFD is used for accelerating the multi-group CMFD calculation has been constructed to improve the calculation efficiency. The newly implemented routines are written in the form of a static library of FORTRAN90 that forms link to the PARCS code during compilation. The new numerical method has been evaluated over benchmark problems for steady-state and transient calculations of real-size reactor core. The calculation results show an excellent agreement with the reference results of the benchmark problem. The computing time of the new routines was about 4 times shorter than that of the original routine.

CONTENTS

	<u>Page</u>
ABSTRACT	iii
CONTENTS	v
LIST OF FIGURES	vii
LIST OF TABLES	ix
EXECUTIVE SUMMARY	xi
FOREWORD	xiii
1. INTRODUCTION	1
2. NUMERICAL METHODOLOGY	3
2.1 Source Expansion Nodal Method.....	3
2.2 Two-Level Coarse Mesh Finite Difference Method	5
2.3 Pin Power Reconstruction With Source Expansion	7
2.3.1 Source Expansion	10
2.3.2 Determination of Corner Flux	13
2.3.3 Corner Discontinuity Factor	14
2.3.4 Reconstruction of Calculation Flow	14
3. IMPLEMENTATION	17
3.1 SENM Library.....	17
3.1.1 MAIN.....	17
3.1.2 BICG.....	19
3.1.3 CMFD	20
3.1.4 SENM2N.....	20
3.1.5 PPR.....	20
3.1.6 TRAN.....	20
3.2 Modification of PARCS code	21
4. VERIFICATION	23
4.1 Part I – 2D calculation at Fixed T/H Conditions	23
4.2 Part II – 3D calculation at Hot Full Power Conditions	25
4.3 Part III – 3D calculation at Hot Zero Power Conditions.....	27
4.4 Part IV – 3D transient calculation.....	30
4.5 Computing Time Performance	34

5. CONCLUSIONS	37
6. REFERENCES	39

LIST OF FIGURES

	<u>Page</u>
Figure 1	Two-Level CMFD Calculation Flow8
Figure 2	4 sets of net currents at a corner surrounded by four nodes 13
Figure 3	Categories of the SENM library 17
Figure 4	Flow chart of <i>runsteady</i> 18
Figure 5	Flow chart of <i>runtrans</i> 19
Figure 6	Flow chart of <i>drivesenm2n</i>21
Figure 7	Axial power distribution26
Figure 8	Axial power distribution error26
Figure 9	Axial power distribution at HZP conditions29
Figure 10	Axial power distribution error at HZP conditions29
Figure 11	Transient core power behavior31
Figure 12	Transient assembly peaking factor32
Figure 13	Transient point pin peaking factor.....32
Figure 14	Transient core average Doppler temperature33
Figure 15	Transient core average moderator density33
Figure 16	Transient core average moderator temperature34

LIST OF TABLES

	<u>Page</u>
Table 1	Comparison of eigenvalue and assembly power24
Table 2	Pin power %PWE at ARO24
Table 3	Pin power %EWE at ARO25
Table 4	Comparison of CBC, assembly power and core average T/H properties25
Table 5	Pin power %PWE at HFP27
Table 6	Pin power %EWE at HFP27
Table 7	Comparison of critical boron concentration and assembly power28
Table 8	Pin power %PWE at HZP conditions30
Table 9	Pin power %EWE at HZP conditions30
Table 10	Transient peak power and power integral31
Table 11	Comparison of computing times for the steady-state calculation (Part II)35
Table 12	Comparison of computing time for the transient calculation (Part IV)35

EXECUTIVE SUMMARY

In order to improve the performance of PARCS code for multi-group problems, a new semi-analytic nodal method and a pin power reconstruction method have been developed by introducing the source expansion method. These are named as the source expansion nodal and pin power reconstruction methods. The neutron balance equations are coupled with each other through the fissioning and scattering terms. Therefore, the coupled equations need to be solved simultaneously to obtain the group-wise solutions for all the groups. However, this is burdensome because the calculating performance deteriorates as the number of energy groups increases. The source expansion method enables to avoid simultaneous calculations for solving the group-wise neutron balance equations. This is the reason why the source expansion method is used in this work. The PARCS code modified with the source expansion method has improved its calculating performance without compromising its accuracy.

The calculation procedure of the source expansion nodal method is as follows.

1. The right hand side of the neutron balance equation which consists of fissioning, scattering and transverse leakage terms is approximated by a fourth order polynomial function based on the Legendre polynomial. In the initial calculation, the shape of the polynomial function can be flattened by using the average flux value which is determined by finite difference calculation.
2. Once the right hand side becomes a known value, the neutron balance equation can be solved with the proper boundary conditions. The average flux of two neighbored nodes and the flux and current continuities at the interface of those nodes are used as the constraints in determining the homogeneous solutions.
3. The steps 1 and 2 are repeated for all energy groups to determine the group-wise general solutions.
4. The general solution is expanded to a fourth order polynomial function with the orthogonal expansion using the least square method.
5. The right hand side is updated using all of the group-wise expanded solutions.
6. The steps from 1 to 5 are repeated until the intra-nodal shape of fission source is converged. Then, the group-wise exact solutions of the neutron balance equation are obtained.

The final solution by the source expansion nodal method with sufficient iterations becomes essentially identical to the solution by simultaneous calculation. The source expansion pin power reconstruction method also follows the same procedure of the source expansion nodal method except determining the homogeneous solution with the 8 boundary conditions; 4 surface currents and 4 corner fluxes of each node.

A PWR MOX/UO₂ core benchmark problem has been used as the reference in order to evaluate the new source expansion kernel of the PARCS code. In all parts of the problem including steady-state and transient cases, the new source expansion kernel provided quite good accuracy compared to the original nodal expansion kernel. Especially, the multi-group pin power results which are not obtainable with the original kernel have become available with the new source expansion kernel and agrees well with the reference. The source expansion kernel shows a calculation performance about 4 times faster than the nodal expansion kernel for the 3D real-size core problems. The newly implemented source expansion kernel has provided a great accuracy, yet very fast speed regardless structure of energy groups chosen.

FOREWORD

This report represents one of the code improvement submitted to fulfill the bilateral agreement for cooperation in thermal-hydraulic activities between Korean Institute of Nuclear Safety (KINS) and the U.S. Nuclear Regulatory Commission (NRC) in the form of a Korean contribution to the NRC's Code Assessment and Maintenance Program (CAMP), the main purpose of which is to validate the TRAC/RELAP Advanced Computational Engine (TRACE) Code.

KINS and other participants in Korea have established a coordinated frame called NuSTEP with three objectives: to fulfill the formal CAMP requirements, to keep maintenance and assessment activities for safety analysis codes including the MARS code, and to improve the quality of the technical support groups that provide services to Korean Utilities, KINS, research institutes, and engineering companies.

The NuSTEP Review Committee has reviewed this report as the contribution by KEPCO Nuclear Fuel and Seoul National University to NuSTEP.

1. INTRODUCTION

Although there has been growing interest in the transport based core neutronics analysis methods for more accurate calculation with high performance computers, it is yet impractical to apply them in the real core design activities because their performance is not so great on ordinary desktop or server machines. For this reason, most of the neutronics codes for reactor core calculation are still subject to the two-step calculation procedure which consists of homogenized group constant generation and core diffusion calculation. In the core calculation step which is the main concern of this work, nodal codes based on the diffusion theory have been used to determine the multiplication factor and flux distribution. Practically, almost all nodal codes employ the two-group formulation involving only fast and thermal neutron energy groups for the applications to light water reactors. However, numerical calculations with the two-group structure is not appropriate in the analysis of the cores loaded with mixed oxide fuels or of the fast breed reactors, since the neutron spectrum is influenced more by the core environment requiring much more energy groups than two groups.

The PARCS code [1] is one of the very efficient nodal codes in which the analytic nodal method is implemented within the CMFD formulation. It also employs a unique and accurate two-dimensional analytic solution based pin power reconstruction method. The analytic nodal method and pin power reconstruction solvers are, however, efficient only for two group solution. As an optional solver, PARCS has a nodal expansion method based multi-group nodal solver employing the one-node formulation. But this one-node NEM multi-group solver was not optimized and is too slow to calculate the real-size reactor cores. Furthermore, the pin power reconstruction solver does not support multi-group solutions. It is therefore now planned to add an efficient multi-group calculation capability for both the nodal solution and pin power reconstruction.

Among the several nodal methods, there have been renewed interests in the semi-analytic nodal method [2-6] in the last decade because of the ease of multi-group extension while retaining the level of solution accuracy provided by the analytic nodal method. The source expansion nodal method [6] developed at Korea Nuclear Fuel and Seoul National University is a semi-analytic nodal method and optimized for multi-group calculation such that the source expansion form provides an advantage of decoupling group dependence and the ease of increasing the source expansion order which can reduce calculation time.

As an acceleration method for the nodal calculation, the coarse mesh finite difference (CMFD) formulation [7, 8] is widely used. A two-group CMFD solver was already implemented in PARCS to accelerate the two-group analytic nodal kernel and also the multi-group nodal expansion kernel. In the multi-group nodal expansion kernel which is based on the one-node scheme, the incoming partial currents are specified at the surfaces of a node of interest as the boundary condition and the one-dimensional flux shape in each direction is determined so that the node average flux and the outgoing partial currents can be newly determined. Therefore, the multi-group spectrum within a node can be updated by the one-node nodal calculation and the CMFD calculation is only used as an acceleration scheme. On the contrary, the two-node scheme has been chosen for the multi-group source expansion nodal method primarily because the two-node scheme provides better convergence characteristics than the one-node scheme primarily. It is due to that better current vs. node average flux relations can be obtainable from the two-node scheme in which the properties of the both nodes of an interface are reflected simultaneously in the determination of the interface current. However, in the two-node scheme, the node average fluxes of the two nodes are specified as the constraints and the flux shape satisfying the current and flux continuity at the interface of the two nodes as well as the node

average flux constraints is determined. Therefore, a multi-group CMFD solution is inevitable when using the two-node source expansion nodal method. Since the multi-group CMFD calculation converges more slowly than the two-group CMFD calculation because of the source iteration, it would be beneficial to establish a two-group CMFD from the multi-group CMFD to accelerate the multi-group calculation. Then the efficient two-group solution method such as the Wielandt eigenvalue shift method and the simultaneous group solution scheme (as opposed to the groupwise solution scheme) can be utilized.

In this document, the multi-group numerical methodologies are presented in Chapter 2 and their implementation is introduced in Chapter 3. Then, the computational performance of the new implementation is evaluated with a MOX/UO₂ fueled benchmark problem [9] for steady-state and transient cases in Chapter 4.

2. NUMERICAL METHODOLOGY

2.1 Source Expansion Nodal Method

The source expansion nodal method (SENM) is based on the transverse-integrated neutron diffusion equation which can be written as follows in terms of the normalized coordinate variable $\xi_u = 2u / h_u$, where h_u is the node width in the u -direction, with the omission of the subscript u for brevity:

$$-\frac{4D_g}{h^2} \frac{\partial^2 \phi_g(\xi)}{\partial \xi^2} + \Sigma_{rg} \phi_g(\xi) = \frac{\chi_g}{k_{eff}} \psi(\xi) + S_g(\xi) - L_g(\xi), \quad (1)$$

where the right hand side terms representing the fission source ($\chi_g \psi$), scattering source (S_g), and the transverse leakage (L_g), respectively. The origin of the coordinate is the center of the node and thus the range of the normalized coordinate is $[-1, 1]$. This choice of normalization is dictated by the choice of Legendre polynomial $P_i(\xi)$ for the source expansion. It is supposed that the transverse leakage is given by a quadratic polynomial.

In the fourth order source expansion nodal method, the fission and scattering sources are approximated by a quartic polynomial so that the entire right hand side (RHS) of Eq. (1) can be represented as:

$$Q_g(\xi) \equiv \frac{\chi_g}{k_{eff}} \psi(\xi) + S_g(\xi) - L_g(\xi) = \sum_{i=0}^4 q_{gi} P_i(\xi) \quad (2)$$

where $L_g(\xi)$ is given in the form of quadratic polynomial and will be obtained from the leakages over the three adjacent nodes. The source expansion coefficient (q_i) is predetermined with an initial guess or a previous solution which has been approximated by a fourth order polynomial given in Eq. (7).

Given the RHS as a quartic polynomial, the analytic solution of Eq. (1) is obtained as the following:

$$\phi_g(\xi) = \phi_g^H(\xi) + \phi_g^P(\xi) = A_g \sinh(\kappa_g \xi) + B_g \cosh(\kappa_g \xi) + \sum_{i=0}^4 c_{gi} P_i(\xi), \quad (3)$$

where the superscripts H and P stand for the homogeneous and particular solutions, respectively, and $\kappa_g = \frac{h}{2} \sqrt{\frac{\Sigma_{rg}}{D_g}}$.

The coefficients of the particular solution (c_{gi}) are all determined uniquely by the source term coefficients as follow:

$$\begin{aligned}
c_{g0} &= \frac{1}{\Sigma_{rg}} \left(q_{g0} + \frac{1}{\kappa_g^2} (3q_{g2} + 10q_{g4}) + \frac{1}{\kappa_g^4} 105q_{g4} \right), \\
c_{g1} &= \frac{1}{\Sigma_{rg}} \left(q_{g1} + \frac{15}{\kappa_g^2} q_{g3} \right), \quad c_{g2} = \frac{1}{\Sigma_{rg}} \left(q_{g2} + \frac{35}{\kappa_g^2} q_{g4} \right), \\
c_{g3} &= \frac{q_{g3}}{\Sigma_{rg}}, \quad \text{and} \quad c_{g4} = \frac{q_{g4}}{\Sigma_{rg}}.
\end{aligned} \tag{4}$$

Next, the coefficients of the homogeneous solution should be determined by imposing constraints or boundary conditions. In the source expansion nodal method, the even term coefficient of the homogeneous solution, B_g , which is obtained from the node average flux constraint as follows.

$$B_g = \frac{\kappa_g}{\sinh(\kappa_g)} (\bar{\phi}_g - c_{g0}) \tag{5}$$

Now the only unknown coefficient is A_g and it needs to be determined for each node leading to two unknowns per node. These two are determined by solving the following coupled equations which are given by the following flux and current continuity at the interface:

$$\begin{bmatrix} \sinh(\kappa_g^l) & \sinh(\kappa_g^r) \\ 2\beta_g^l \kappa_g^l \cosh(\kappa_g^l) & -2\beta_g^r \kappa_g^r \cosh(\kappa_g^r) \end{bmatrix} \begin{bmatrix} A_g^l \\ A_g^r \end{bmatrix} = \begin{bmatrix} \gamma_\phi \\ \gamma_J \end{bmatrix} \tag{6}$$

where

$$\begin{aligned}
\gamma_\phi &= B_g^r \cosh(\kappa_g^r) - B_g^l \cosh(\kappa_g^l) + \sum_{i=0}^4 ((-1)^i c_{gi}^r - c_{gi}^l) \\
\gamma_J &= -2\beta_g^l (B_g^l \kappa_g^l \sinh(\kappa_g^l) + a_{g1}^l + 3a_{g2}^l + 6a_{g3}^l + 10a_{g4}^l) \\
&\quad - 2\beta_g^r (B_g^r \kappa_g^r \sinh(\kappa_g^r) - a_{g1}^r + 3a_{g2}^r - 6a_{g3}^r + 10a_{g4}^r).
\end{aligned}$$

With the five particular coefficients and the two homogeneous coefficients, the solution given by Eq. (3) is uniquely determined and then the flux shape involving the *sinh* and *cosh* functions can be approximated by a quartic polynomial given by Eq. (7) using the orthogonal property of Legendre polynomials as follows:

$$\phi_g(\xi) \approx \bar{\phi}_g + \sum_{i=1}^4 a_{gi} P_i(\xi) \tag{7}$$

$$\begin{aligned}
a_{gi} &= \frac{\langle \phi_g(\xi), P_i(\xi) \rangle}{\langle P_i(\xi), P_i(\xi) \rangle}, \\
a_{g1} &= c_{g1} + \frac{3}{\kappa_g} \left(\cosh(\kappa_g) - \frac{\sinh(\kappa_g)}{\kappa_g} \right) A_g, \\
a_{g2} &= c_{g2} - 5 \left(\frac{3 \cosh(\kappa_g)}{\kappa_g^2} - \left(1 + \frac{3}{\kappa_g^2}\right) \frac{\sinh(\kappa_g)}{\kappa_g} \right) B_g, \\
a_{g3} &= c_{g3} + \frac{7}{\kappa_g} \left(\left(1 + \frac{15}{\kappa_g^2}\right) \cosh(\kappa_g) - \left(6 + \frac{15}{\kappa_g^2}\right) \frac{\sinh(\kappa_g)}{\kappa_g} \right) A_g, \text{ and} \\
a_{g4} &= c_{g4} - 9 \left(\frac{5}{\kappa_g^2} \left(2 + \frac{21}{\kappa_g^2}\right) \cosh(\kappa_g) - \left(1 + \frac{45}{\kappa_g^2} + \frac{105}{\kappa_g^4}\right) \frac{\sinh(\kappa_g)}{\kappa_g} \right) B_g.
\end{aligned} \tag{8}$$

Here the bracket stands for inner product of the functions involving an integral over [-1,1]. Note that the orthogonal expansion corresponds to the least square fitting of a function based on the weighted residual procedure.

The source expansion nodal method involves a scheme of source iteration. It is thus necessary to establish a proper condition to check the convergence of the multi-group flux solution. Since the change in the flux shape is directly reflected into the fission source shape, the fission source shape within the local nodes can be monitored to check the convergence. Instead of checking fission source convergence, it is also possible to check convergence of individual group fluxes. But that kind of strict convergence check is not necessary because the source level and shape keep changing during the outer iteration. Specifically, the following convergence parameter is used in the source expansion nodal method:

$$\delta^{(n+1)} = \frac{1}{\bar{\psi}^{(n+1)}} \left(\frac{1}{2} \int_{-1}^1 (\psi^{(n+1)}(\xi) - \psi^{(n)}(\xi))^2 d\xi \right)^{1/2} \tag{9}$$

with n being the source iteration index.

By expanding the fission source into a quartic polynomial using Legendre polynomials and using the orthogonal property of the Legendre polynomials, the above integral can be reduced as follows:

$$\delta^{(n+1)} = \frac{1}{\bar{\psi}^{(n+1)}} \left(\sum_{i=0}^4 \frac{1}{2i+1} (q_{\psi i}^{(n+1)} - q_{\psi i}^{(n)})^2 \right)^{1/2}, \tag{10}$$

where $q_{\psi i}^{(n)}$ is the i -th order fission source expansion coefficient at iteration step n . In case of non-fuel nodes, the fission source is replaced with the lowest energy group flux.

2.2 Two-Level Coarse Mesh Finite Difference Method

There can be two views of the coarse mesh finite difference (CMFD) formulation which employs a correction term in the current vs. node average flux relation. The first view is to regard the

CMFD as an acceleration scheme for the higher order methods whereas the second view is to regard it as a complete nodal balance formulation employing higher order current relations. The latter view enables more extensive and efficient application of the CMFD formulation to various problems. For instance, a CMFD standalone spatial kinetics calculation is possible by applying a suitable temporal differencing to the CMFD balance equations. In this case, only occasional updates of the higher order correction factors are required and the correction factor appearing in the current vs. node average flux relation can be obtained by solving the local problem with the source expansion nodal method.

Suppose that multi-group surface currents are specified for the local problem like the source expansion nodal calculation. It is then possible to define the current correction factor such as:

$$\hat{D}_g = -\frac{\tilde{D}_g(\bar{\phi}_g^r - \bar{\phi}_g^l) + J_g}{\bar{\phi}_g^r + \bar{\phi}_g^l} \quad (11)$$

where the superscripts, l and r , denote the left and right nodes, respectively, J_g is the surface current, and \tilde{D}_g is the finite difference method (FDM) based proportional constant relating the current to the flux difference defined as:

$$\tilde{D}_g = \frac{2D_g^r D_g^l}{h(D_g^r + D_g^l)}.$$

The multi-group CMFD calculation can be performed to update globally the node average fluxes with the correction factor. However, the convergence of the multi-group calculation is generally slower than the corresponding two-group problem because of the ineffectiveness of the source iteration scheme. For instance, the Chebyshev acceleration scheme employed in the multi-group eigenvalue problem shows an inferior performance to the Wielandt eigenvalue shift method which is readily employed in a two-group problem. This motivates a dynamic two-group formulation during the multi-group CMFD calculation.

Once the multi-group node average fluxes and surface currents are available from the multi-group CMFD calculation, it is then possible to define the corresponding two-group cross section and the current correction factor as follows:

$$\Sigma_{\alpha\hat{g}} = \sum_{g \in S_{\hat{g}}} \Sigma_{\alpha g} \varphi_g, \quad (12)$$

$$\hat{D}_g = -\frac{\tilde{D}_g(\bar{\phi}_g^r - \bar{\phi}_g^l) + J_g}{\bar{\phi}_g^r + \bar{\phi}_g^l} \quad (13)$$

where \hat{g} is the coarse group index, α is the reaction type, and

$$\varphi_g = \frac{\bar{\phi}_g}{\bar{\phi}_{\hat{g}}}, \quad \bar{\phi}_{\hat{g}} = \sum_{g \in S_{\hat{g}}} \bar{\phi}_g, \quad J_g = \sum_{g \in S_{\hat{g}}} J_g \quad (\hat{g} = 1, 2).$$

Here $S_{\hat{g}}$ designates the set of the fine group number belonging to coarse group \hat{g} . The coarse

group current correction is used in the two-group CMFD formulation to relate the interface current with the two node average fluxes of the interface as follows:

$$J_{\hat{g}} = -\tilde{D}_g(\bar{\phi}_g^r - \bar{\phi}_g^l) - \hat{D}_g(\bar{\phi}_g^r + \bar{\phi}_g^l) \quad (14)$$

Once the two-group CMFD calculation is performed, the two-group node average flux distribution becomes available and is used to adjust the multi-group fluxes with the multi-group intra-node spectrum stored in the previous multi-group calculation. The subsequent multi-group CMFD calculation is done once again to update the solution satisfying the nodal balance equation with the expanded multi-group fluxes. Then, the source expansion nodal calculation is repeated with the updated average fluxes.

This overall flow of two level CMFD calculation involving two-group and multi-group CMFD solutions is depicted in Fig. 1. As seen in the flow chart, there are several decision points in the two-level CMFD calculation. First, the overall convergence check is made only once per nodal update cycle. It is done at the first MG CMFD group sweep performed right after each nodal update. This is to make sure that the overall convergence is achieved even after the nodal update. The exit from the MG CMFD to 2G CMFD is made when sufficient residual error reduction is achieved. The exit from the 2G CMFD to MG CMFD is also made after certain residual reduction during the 2G calculation. The exit from the MG to the nodal update is made at the first MG CMFD after a 2G CMFD calculation.

2.3 Pin Power Reconstruction With Source Expansion

After integrating the three-dimensional neutron diffusion equation axially over a plane of thickness, h_z , the following two-dimensional balance equation is obtained for each group with all the source terms placed on the right hand side (RHS).

$$-D_g \nabla^2 \phi_g(x, y) + \Sigma_{rg} \phi_g(x, y) = \frac{1}{k_{eff}} \chi_g \sum_{g'} \nu \Sigma_{fg'} \phi_{g'}(x, y) + \sum_{g' \neq g} \Sigma_{g'g} \phi_{g'}(x, y) - L_{gz}(x, y) \quad (15)$$

where the axial transverse leakage is defined as $L_{gz}(x, y) = (J_{gz}^T(x, y) - J_{gz}^B(x, y)) / h_z$ in term of the currents at the top and bottom surfaces of the plane and k_{eff} is the multiplication factor. The entire RHS terms can be approximated by a polynomial of two spatial coordinate variables. The polynomial for a two-dimensional shape is iteratively updated. With such a polynomial approximation, the solution of Eq. (15) would be obtained straight forwardly for a square node whose width is h .

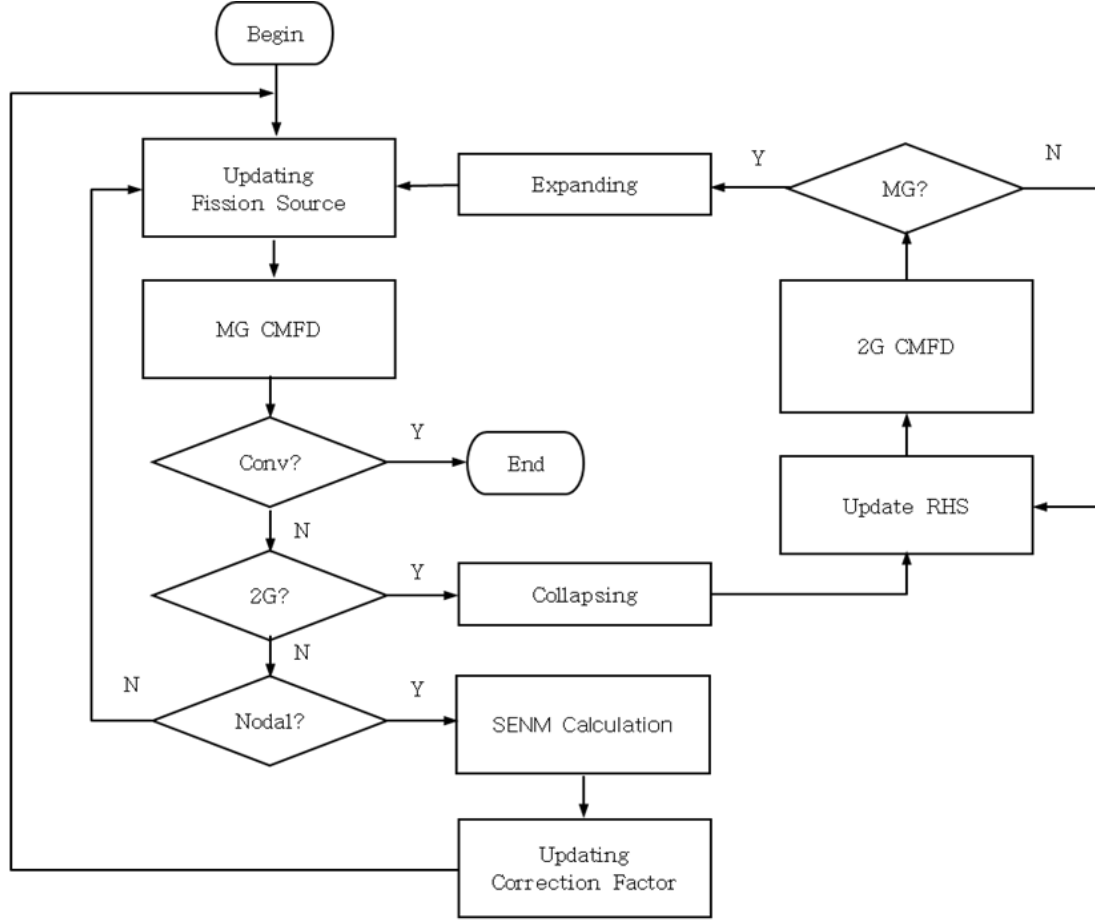


Figure 1 Two-Level CMFD Calculation Flow

Since it is advantageous to use the Legendre polynomial for the polynomial approximation owing to its orthogonality property, we first normalize the independent variable such that it varies from -1.0 to 1.0 in the node. This leads to the following equation with the group index g omitted:

$$-\frac{4D}{h^2} \left(\frac{\partial^2}{\partial \xi^2} + \frac{\partial^2}{\partial \eta^2} \right) \phi(\xi, \eta) + \Sigma_r \phi(\xi, \eta) = Q(\xi, \eta) \quad (16)$$

where $\xi = 2x/h$, $\eta = 2y/h$, and $Q(\xi, \eta)$ represents the distribution of the entire sources. As an approximation for the source distribution, we use a quartic polynomial given in terms of Legendre polynomials:

$$Q(\xi, \eta) = \sum_{\substack{i=0 \\ i+j \leq 4}}^4 \sum_{j=0}^4 q_{i,j} P_i(\xi) P_j(\eta) \quad (17)$$

where $P_i(\xi)$ is the i -th order Legendre polynomial. Note that this 15-term polynomial contains

fourth order cross terms such as $P_1(\xi)P_3(\eta)$ and $P_2(\xi)P_2(\eta)$ representing a quartic variation in each direction. In the following, it is assumed that the source term coefficients are known and so are the 8 boundary conditions for each group.

The solution of the non-homogeneous second order differential equation, Eq. (16), consists of the homogeneous and particular solutions. The particular solution has the same functional form as the source polynomial, Eq. (17). The coefficients, $p_{i,j}$, of the polynomial particular solution, $\phi_p(\xi, \eta)$, can be determined by the method of undetermined coefficient as follows.

$$\begin{aligned}
p_{0,0} &= \frac{48D^2(35(q_{0,4} + q_{4,0}) + 6q_{2,2})}{h^4\Sigma_r^3} + \frac{4D(3(q_{0,2} + q_{2,0}) + 10(q_{0,4} + q_{4,0}))}{h^2\Sigma_r^2} + \frac{q_{0,0}}{\Sigma_r}, \\
p_{0,1} &= \frac{12D(5q_{0,3} + q_{2,1})}{h^2\Sigma_r^2} + \frac{q_{0,1}}{\Sigma_r}, \quad p_{1,0} = \frac{12D(5q_{3,0} + q_{1,2})}{h^2\Sigma_r^2} + \frac{q_{1,0}}{\Sigma_r}, \\
p_{0,2} &= \frac{D(12q_{2,2} + 140q_{0,4})}{h^2\Sigma_r^2} + \frac{q_{0,2}}{\Sigma_r}, \quad p_{2,0} = \frac{D(12q_{2,2} + 140q_{4,0})}{h^2\Sigma_r^2} + \frac{q_{2,0}}{\Sigma_r}, \\
p_{i,j} &= \frac{q_{i,j}}{\Sigma_r} \text{ for other (i,j) combinations.}
\end{aligned} \tag{18}$$

The homogeneous equation of Eq. (16) can be rewritten by dividing by $4D/h^2$ as follows:

$$\left(\frac{\partial^2}{\partial \xi^2} + \frac{\partial^2}{\partial \eta^2} \right) \phi(\xi, \eta) = B_t^2 \phi(\xi, \eta) \tag{19}$$

where the dimensionless buckling is defined as:

$$B_t^2 = \frac{h^2\Sigma_r}{4D} = \frac{h^2}{4L^2} \text{ or } B_t = \frac{h}{2L} \tag{20}$$

with L being the diffusion length. Eq. (19) can be solved by separation of variables after splitting the total buckling as follows:

$$B_t^2 = B_{t,\xi}^2 + B_{t,\eta}^2 \tag{21}$$

where $B_{t,\xi} = B_t \cos \theta$ and $B_{t,\eta} = B_t \sin \theta$. There are infinite numbers of splittings by Eq. (21) and the solution satisfying the boundary condition at all the boundary points can be obtained in terms of an infinite series. However, we choose only eight pairs with the following angles which would require only 8 boundary conditions:

$$\theta_k = \frac{\pi}{4}k, \quad k = 0..7 \tag{22}$$

This leads to the following form of the homogeneous equation:

$$\phi_H(\xi, \eta) = \sum_{k=0}^7 \hat{a}_k e^{B_i(\xi \cos \theta_k + \eta \sin \theta_k)} \quad (23)$$

which can be rewritten in terms of *sinh* and *cosh* as:

$$\begin{aligned} \phi_H(\xi, \eta) = & a_1 \sinh(B_i \xi) + a_2 \cosh(B_i \xi) + a_3 \sinh(B_i \eta) + a_4 \cosh(B_i \eta) \\ & + a_5 \sinh\left(\frac{B_i \eta}{\sqrt{2}}\right) \cosh\left(\frac{B_i \eta}{\sqrt{2}}\right) + a_6 \sinh\left(\frac{B_i \xi}{\sqrt{2}}\right) \sinh\left(\frac{B_i \eta}{\sqrt{2}}\right) \\ & + a_7 \cosh\left(\frac{B_i \eta}{\sqrt{2}}\right) \sinh\left(\frac{B_i \eta}{\sqrt{2}}\right) + a_8 \cosh\left(\frac{B_i \xi}{\sqrt{2}}\right) \cosh\left(\frac{B_i \eta}{\sqrt{2}}\right) \end{aligned} \quad (24)$$

The four surface average currents and four corner fluxes are chosen as the boundary conditions to determine the eight coefficients of Eq. (24). The reason for choosing the four surface average current as the boundary condition is to force that the average of the 2D flux solution over the node be exactly the same as the one determined in the 3D nodal calculation. This is possible because the nodal solution and the two-dimensional solution satisfy the nodal balance equation involving the same surface average currents.

2.3.1 Source Expansion

In deriving the eight homogeneous solution coefficients, it is convenient to make the boundary condition apply only to the homogeneous solution by subtracting the particular solution part from the whole boundary condition. This is because the particular solution is always determined uniquely once the source polynomial is specified. For example, the homogenous part of the flux at the northwest corner ($\xi = -1, \eta = 1$) is obtained as follows:

$$\begin{aligned} \phi_{NW}^H &= \phi_{NW} - \phi_{NW}^P \\ &= \phi_{NW} - (p_{0,0} + p_{0,1} + p_{0,2} + p_{0,3} + p_{0,4} - p_{1,0} \\ &\quad + p_{2,0} - p_{3,0} + p_{4,0} - p_{1,1} - p_{1,2} + p_{2,1} + p_{2,2}) \end{aligned} \quad (25)$$

And the surface average current at the west surface is given by:

$$\begin{aligned} \bar{J}_{x,l}^H &= \bar{J}_x^l - \frac{1}{2} \int_{-1}^1 J_x^P(-1, \eta) d\eta \\ &= \bar{J}_x^l + \frac{2D}{h} (p_{1,0} - 3p_{2,0} + 6p_{3,0} - 10p_{4,0}) \end{aligned} \quad (26)$$

where the superscript *l* designates the left surface and the current for the particular solution part is given by:

$$J_x^P(\xi, \eta) = -\frac{2D}{h} \frac{\partial \phi_P(\xi, \eta)}{\partial \xi} \quad (27)$$

The corner flux at other corner points and the surface average current at other surfaces for the homogeneous solution component can be obtained similarly.

In terms of these boundary conditions for the homogeneous solution, the coefficients are determined as follows:

$$\begin{aligned}
a_1 &= \frac{B_t h J_{x,s}^H + 2D\phi_1^H}{2D(S - B_t C)}, \quad a_2 = -\frac{B_t h J_{x,d}^H + 2DS^2 a_8}{2D_g S_g B_{t,g}}, \\
a_3 &= \frac{B_t h J_{y,s}^H + 2D\phi_3^H}{2D(S - B_t C)}, \quad a_4 = -\frac{B_t h J_{y,d}^H + 2DS^2 a_8}{2DSB_t}, \\
a_5 &= \frac{B_t (hS J_{x,s}^H + 2CD\phi_1^H)}{2D(B_t C - S)\tilde{X}}, \quad a_6 = \frac{\phi_2^H}{S^2}, \\
a_7 &= \frac{B_t (hS J_{y,s}^H + 2CD\phi_3^H)}{2D(B_t C - S)\tilde{X}}, \\
a_8 &= \frac{B_t (Ch(J_{x,d}^H + J_{y,d}^H) + 2DS\phi_4^H)}{2D(B_t SC^2 - 2CS^2)},
\end{aligned} \tag{28}$$

where

$$\begin{aligned}
S &= \sinh(B_t), \quad \tilde{S} = \sinh\left(\frac{B_t}{\sqrt{2}}\right), \\
C &= \cosh(B_t), \quad \tilde{C} = \cosh\left(\frac{B_t}{\sqrt{2}}\right), \\
\tilde{X} &= S^2 \times C^2,
\end{aligned}$$

$$\begin{bmatrix} J_{x,s}^H \\ J_{x,d}^H \\ J_{y,s}^H \\ J_{y,d}^H \end{bmatrix} = \frac{1}{2B_t} \begin{bmatrix} \bar{J}_{x,r}^H + \bar{J}_{x,l}^H \\ \bar{J}_{x,r}^H - \bar{J}_{x,l}^H \\ \bar{J}_{y,r}^H + \bar{J}_{y,l}^H \\ \bar{J}_{y,r}^H - \bar{J}_{y,l}^H \end{bmatrix}$$

and

$$\begin{bmatrix} \phi_1^H \\ \phi_2^H \\ \phi_3^H \\ \phi_4^H \end{bmatrix} = \frac{1}{4} \begin{bmatrix} \phi_{NE}^H - \phi_{NW}^H + \phi_{SE}^H - \phi_{SW}^H \\ \phi_{NE}^H - \phi_{NW}^H - \phi_{SE}^H + \phi_{SW}^H \\ \phi_{NE}^H + \phi_{NW}^H - \phi_{SE}^H - \phi_{SW}^H \\ \phi_{NE}^H + \phi_{NW}^H + \phi_{SE}^H + \phi_{SW}^H \end{bmatrix}.$$

The coefficients given by Eqs. (18) and (28) for the particular and homogeneous solutions, respectively, complete the final solution of:

$$\phi(\xi, \eta) = \phi_H(\xi, \eta) + \phi_P(\xi, \eta). \quad (29)$$

In the above derivation, it was assumed that the source distribution is known and describable by a quartic polynomial. With the new 2D solution flux solution available, the primary source distribution which consists of the fission and scattering sources should be updated for use in the next step of the iterative solution sequence. Since the 2D flux distribution for each group contains the exponential function components as well as the polynomial function components whereas the source is to be approximated by only a polynomial function, it is necessary to obtain first the 2D quartic polynomial approximation of the flux distribution for each group. Then the source term coefficients can be obtained by multiplying the flux coefficients by the proper cross section and then by summing over the groups.

As a method for approximating the 2D flux distribution, the least square fitting which makes use of the orthogonal expansion of an analytic function in terms of the Legendre function is employed. The expansion coefficients can be given by:

$$\begin{aligned} c_{i,j} &= \frac{\int_{-1}^1 \int_{-1}^1 \phi(\xi, \eta) P_i(\xi) P_j(\eta) d\xi d\eta}{\int_{-1}^1 \int_{-1}^1 P_i^2(\xi) P_j^2(\eta) d\xi d\eta} \\ &= \frac{1}{4} (2i+1)(2j+1) \int_{-1}^1 \int_{-1}^1 \phi(\xi, \eta) P_i(\xi) P_j(\eta) d\xi d\eta \end{aligned} \quad (30)$$

In Eq. (16), the semi-analytic form of the flux solution, Eq. (29) is to be inserted in the integrand and the integral is trivial. Since it is cumbersome to present all the 15 coefficients here, only the fourth order term is given below:

$$\begin{aligned} c_{4,0} &= 9 \left(\frac{105S}{B_t^4} - \frac{105C}{B_t^3} + \frac{45S}{B_t^2} - \frac{10C}{B_t} + S \right) a_2 \\ &\quad + \frac{18\tilde{S}}{B_t^2} \left(\frac{420\tilde{S}}{B_t^4} - \frac{210\sqrt{2}\tilde{C}}{B_t^3} + \frac{90\sqrt{2}\tilde{S}}{B_t^2} - \frac{10\sqrt{2}\tilde{C}}{B_t} + \tilde{S} \right) a_8 + p_{4,0}. \end{aligned} \quad (31)$$

Once the coefficients of the polynomial flux are updated, the source coefficients can be determined by summing the groupwise source terms:

$$q_{i,j}^g = \frac{\chi_g}{k_{eff}} \sum_{g'} \nu \Sigma_{fg'} c_{i,j}^{g'} + \sum_{g' \neq g} \Sigma_{g'g} c_{i,j}^{g'} - l_{i,j}^g. \quad (32)$$

The updated source coefficients will be used to determine the new particular solution at the next iteration step.

2.3.2 Determination of Corner Flux

Suppose that the two outgoing currents are known at the interface of two nodes in a one-dimensional problem as follows:

$$J_1^+ = \frac{1}{4}\phi_s + \frac{1}{2}J_1^{net} \text{ and } J_2^+ = \frac{1}{4}\phi_s - \frac{1}{2}J_2^{net}. \quad (33)$$

Here the numeric subscripts indicate the node number. Node 1 is for left node and 2 is for the right node. It is assumed that the net currents determined at the two nodes are not the same because the current continuity condition is not imposed. With the two outgoing currents, we can determine the new surface flux as follows:

$$\phi_s^{new} = 2(J_1^+ + J_2^+) = \phi_s + (J_1^{net} - J_2^{net}). \quad (34)$$

The equation above states that the new surface flux increases by the difference in the net current.

Now consider a corner surrounded by four nodes as shown in Fig. 2.

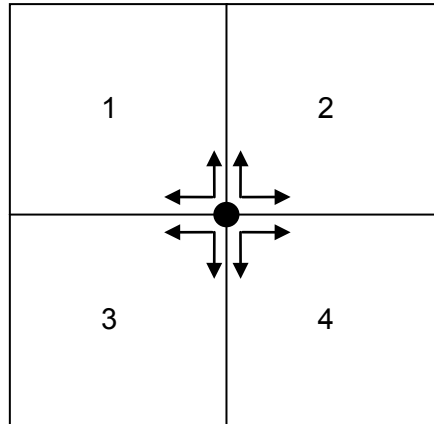


Figure 2 4 sets of net currents at a corner surrounded by four nodes

From the 2D flux solution of each node, x- and y-directional net currents at the corner become available. For the four nodes, there are 4 sets of x- and y-directional currents. In principle, the four x-directional currents must be the same. But since no corner current continuity condition is imposed, there can be difference in the net currents. Using the four sets of net current difference, four estimates of the new corner flux can be obtained by using Eq. (34). By taking the average of the four, the new corner flux is obtained as:

$$\phi_c^{new} = \phi_c + \frac{1}{4}(J_{1,x}^{net} - J_{2,x}^{net} + J_{3,x}^{net} - J_{4,x}^{net} + J_{1,y}^{net} - J_{3,y}^{net} + J_{2,y}^{net} - J_{4,y}^{net}). \quad (35)$$

This iterative update scheme will converge if the summation of the net current differences vanishes, which is the corner point balance condition.

2.3.3 Corner Discontinuity Factor

In the nodal calculation, the assembly discontinuity factor is used to allow discontinuity of homogeneous flux shapes in order to preserve the current of the heterogeneous configuration. This discontinuity must be incorporated when determining the corner fluxes primarily because the nodal flux solution is discontinuous at the interfaces. However, there should be given another consideration for the discontinuity. That is related with the subsequent multiplication of heterogeneous form factors to the homogeneous flux shape to reflect intra-assembly heterogeneity. Let the discontinuity factor which would correspond to the form factor at the corner be ζ_i for assembly i . Then the heterogeneous flux at the corner is obtained by multiplying the corner discontinuity factor (CDF) to the homogeneous flux at the corner. Namely,

$$\phi_c^{het} = \zeta_i \phi_{c,i}^{hom}. \quad (36)$$

Since the heterogeneous flux is supposed to be continuous, the homogeneous flux should be discontinuous.

Once the common corner flux is determined by Eq. (35), we can take that as the heterogeneous corner flux and the homogeneous corner flux for each assembly is determined by dividing it by the CDF. The homogeneous corner flux is then used in Eq. (28).

2.3.4 Reconstruction of Calculation Flow

The pin power reconstruction is to be performed after the multi-group transverse-integrated nodal solution is obtained. The basic information available for each node from the nodal calculation consists of one node average flux, four surface average fluxes, and four surface average currents. The reconstruction starts with this information to determine the homogeneous flux shape with 2D source expansion nodal method (SENM) presented in the previous section. Repeated 2D SENM calculations are needed to update the corner fluxes and the source expansion iteratively. The heterogeneous pin power distribution is finally constructed by multiplying the heterogeneous form factor to the homogeneous flux distribution. This reconstruction procedure is explained with a little more details below.

The initial corner flux can be derived by employing the method of successive smoothing (MSS)[10] which yields the following expression for the corner flux:

$$\phi_c = \bar{\phi}_s^x + \bar{\phi}_s^y - \bar{\phi} \quad (37)$$

where $\bar{\phi}_s^u$ is the surface average flux for the u -directional edge from the corner and $\bar{\phi}$ is the node average flux. Another approximation of the corner flux is possible by simply expressing the 2-D flux distribution with a product of the two one-dimensional fluxes (x and y). This yields with the proper normalization:

$$\phi_c = \frac{\bar{\phi}_s^x \bar{\phi}_s^y}{\bar{\phi}}. \quad (38)$$

Note that Eq. (37) can potentially yield a negative flux while Eq. (38) cannot. Since the MSS estimate would give a better estimate than the latter one in which the cross term effect is totally

neglected, we use Eq. (37) as the default formula for the initial corner flux, but switch to Eq. (38) if the MSS estimate becomes negative. For each corner, normally four estimates of the corner flux value are available, one from each node surrounding the corner. The final corner flux is determined by merely averaging the four available estimates.

With the four corner flux information, there are now 13 pieces of information available for each node. The initial source shape can be determined by fitting these values with a 13 term polynomial. This 13 term polynomial is constructed by omitting the two fourth order cross terms of $P_3(\xi)P_1(\eta)$ and $P_1(\xi)P_3(\eta)$.

Once the source expansion and corner fluxes are determined for each group, it is now possible to determine newly the 15 particular solution coefficients and then the 8 homogeneous solution coefficients for each node and each group. The iterative calculation to update the corner flux and the source expansion coefficients proceed with the iteration scheme shown in Fig. 2. In the practical applications, it turned out that the initial guess of the corner fluxes given by Eq. (37) or (38) are sufficiently accurate so that only about 5 iterations are enough to obtain converged corner fluxes as well as the converged source expansion coefficients.

Once the converged homogeneous flux distribution is obtained, the pinwise flux distribution can be obtained for the homogenized node. The heterogeneity within the node is then reflected by multiplying the groupwise power form factor to the groupwise flux.

3. IMPLEMENTATION

The multi-group solution is implemented by modification of the PARCS code and new addition of routines regarding the multi-group solutions in the form of a static library, namely source expansion nodal method (SENM) library. The SENM library contains various Fortran90 modules for determining node-wise flux distribution during two-group and multi-group steady-state and transient calculations with fixed group constants by use of the source expansion nodal method based on coarse method finite difference (CMFD) formulation. The Wieland shift method is employed to achieve fast fission source convergence by accelerating two-group CMFD calculation. And the multi-group CMFD calculation is accelerated by two-group CMFD calculation with condensed two-group constants. In addition, the bi-conjugate gradient stabilized (BICGSTAB) method with blockwise and pointwise incomplete LU precondition technologies is implemented to solve fixed source problems. Modification of PARCS to integrate the library was confined to input handling and calling driver routines of the library.

3.1 SENM Library

Variables and subroutines of the SENM library are categorized into six sets shown in the following figure in terms of functionalities and each set is composed of several modules in FORTRAN90.

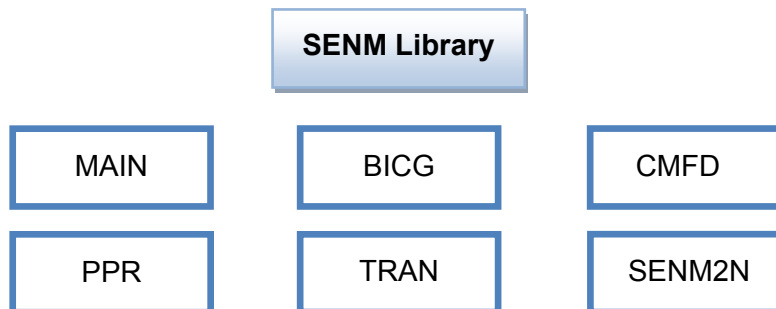


Figure 3 Categories of the SENM library

3.1.1 MAIN

This first category contains eight Fortran90 modules in which numerous subroutines and variables corresponding to the geometry, cross-sections and solutions exist. Several subroutines in this category are opened by calls from PARCS while the other categories are encapsulated. For managing the memory of the computer and avoiding inadvertent memory copies, most of the variables are declared as *POINTER* that can be point variables belonging to PARCS without duplicating memory allocations and initialized when the subroutine, *initvar*, is called.

Among all of the modules, the main module *senm* serves as the main driver routine for steady and transient calculations and calls *runsteady* and *runtrans*. Once the cross-sections are

calculated incorporating the changes in the boron and thermal-hydraulic conditions in PARCS, the driving subroutines, *runsteady* and *runtrans*, are called for one-step of steady and transient calculations, respectively. These determine the average flux distribution, surface current and flux as the results of the CMFD calculations. The following flow charts show the calling sequence of the subroutines in the drivers. In case of two-group problems, only the two-group CMFD calculation is executed for the efficient calculation and an argument to determine to drive the nodal scheme is provided. Convergence check is made through the relative l2 norm of fission source.

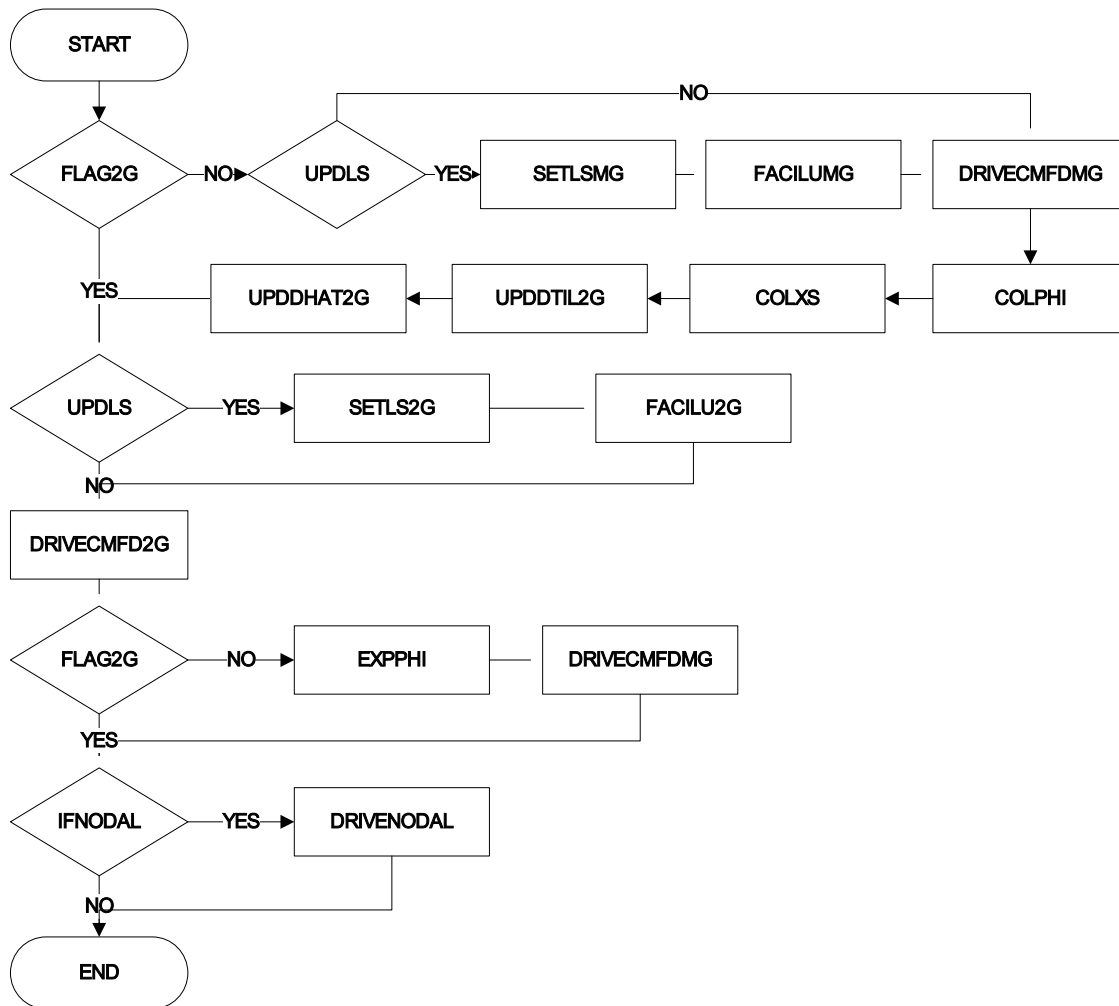


Figure 4 Flow chart of *runsteady*

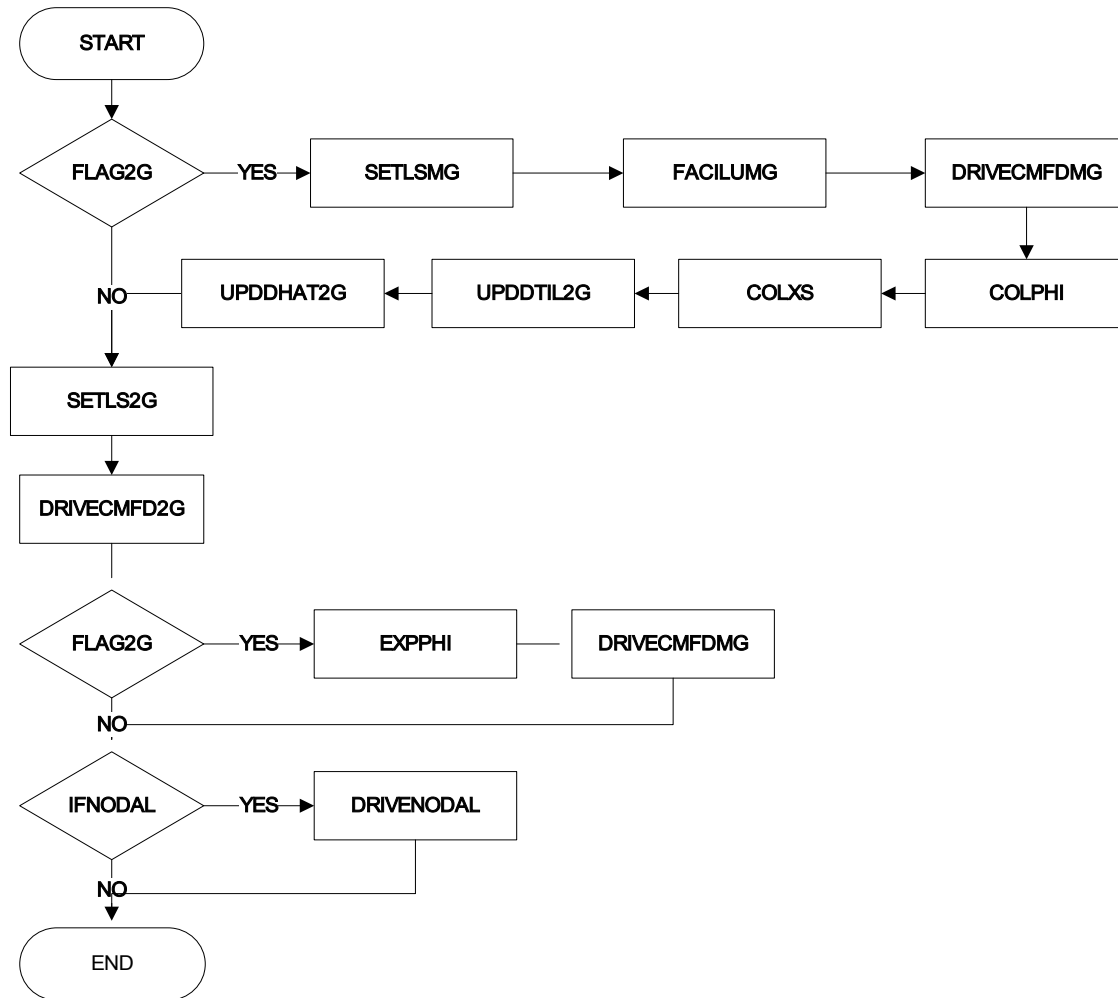


Figure 5 Flow chart of *runtrans*

3.1.2 BICG

The BICG method stands for *Bi-Conjugate Gradient Stabilized method* and this method was implemented for solving two-group and multi-group fixed source problems with fully optimized routines in this category. There are two modules; *bicg2g* and *bicgmg*. In case of two-group problems, the fixed source problem is represented by the blockwise matrix-vector form in which the matrix has N by N block elements and each block element is a 2 by 2 matrix representing group coupling. The module, *bicg2g*, provides several subroutines to solve the fixed source problem with BICGSTAB preconditioned by blockwise incomplete LU technique. The other module, *bicgmg*, is also a linear system solver but has point elements, not block elements, since the linear system is constructed for only one energy group and a scheme of source iterations are employed to consider group-coupling by fission and up-scattering sources. Moreover, the point-wise incomplete LU factorization is used for accelerating BICGSTAB in case of the multi-group solver.

Among the subroutines of *bicg2g*, *facilu2g* and *solbicg2g* called from the module *cmfd2g*, the subroutine *facilu2g* factorize the matrix into incomplete LU with block elements. By looping over rows, the incomplete LU factorization is performed for matrices according to each row and inverse matrices for which the variables *del*, *al* and *au* were used are obtained.

3.1.3 CMFD

This category provides all functionalities solving steady-state and transient problems with the CMFD formulation, in which there are two modules, *bicg2g* and *bicgmg*. These modules consist of four main subroutines: *upddtil2g(mg)*, *upddhat2g(mg)*, *setls2g(mg)* and *drivecmf2g(mg)*. Additionally, the subroutine *wiel* is provided for two-group CMFD calculation for accelerating the calculation with the Wielandt Shift method.

3.1.4 SENM2N

The only module *senm2n* in this category is a Fortran90 module providing subroutines and local variables for calculating the transverse integrated one-dimensional neutron balance equation with the source expansion nodal method. The driving subroutine *drivesenm2n* calls a set of local subroutines in the module sequentially as shown in the following flow chart and determines net current and flux at each surface of all nodes.

3.1.5 PPR

The source expansion pin power reconstruction with multi-group structure was implemented in this category and there is a main module *ppr* that contains a set of subroutines. The module does determine the homogeneous pin power distribution only and not heterogeneous pin power distribution which is calculated by multiplying the heterogeneous form function to the homogeneous pin power distribution. Instead, PARCS determines the heterogeneous one using the homogeneous one provided by the SENM library. It is a proper programming approach to do so because the SENM library does not need to know the heterogeneous form function. The subroutine *ppr* is composed of *initppr*, *calhomo* and *calpinpow*.

3.1.6 TRAN

All modules of the category, TRAN, are materials for the multi-group transient calculation and used in the subroutine *runtrans*. Several subroutines for initializing, subsets of transient calculations and numerous variables represent kinetic parameters and pre-calculated values in the modules; *tranxsec* and *tran*. The first module is *tranxsec* which provides variables corresponding to additional group constants needed for the transient calculation such as delayed neutron parameters. And the subroutine, *malloctranxsec*, has a role of allocating memories for the variables. This subroutine uses the memory sharing technique to avoid duplicate memory allocation by PARCS. The other module *tran* is a main module to provide subroutines to calculate transient parameters.

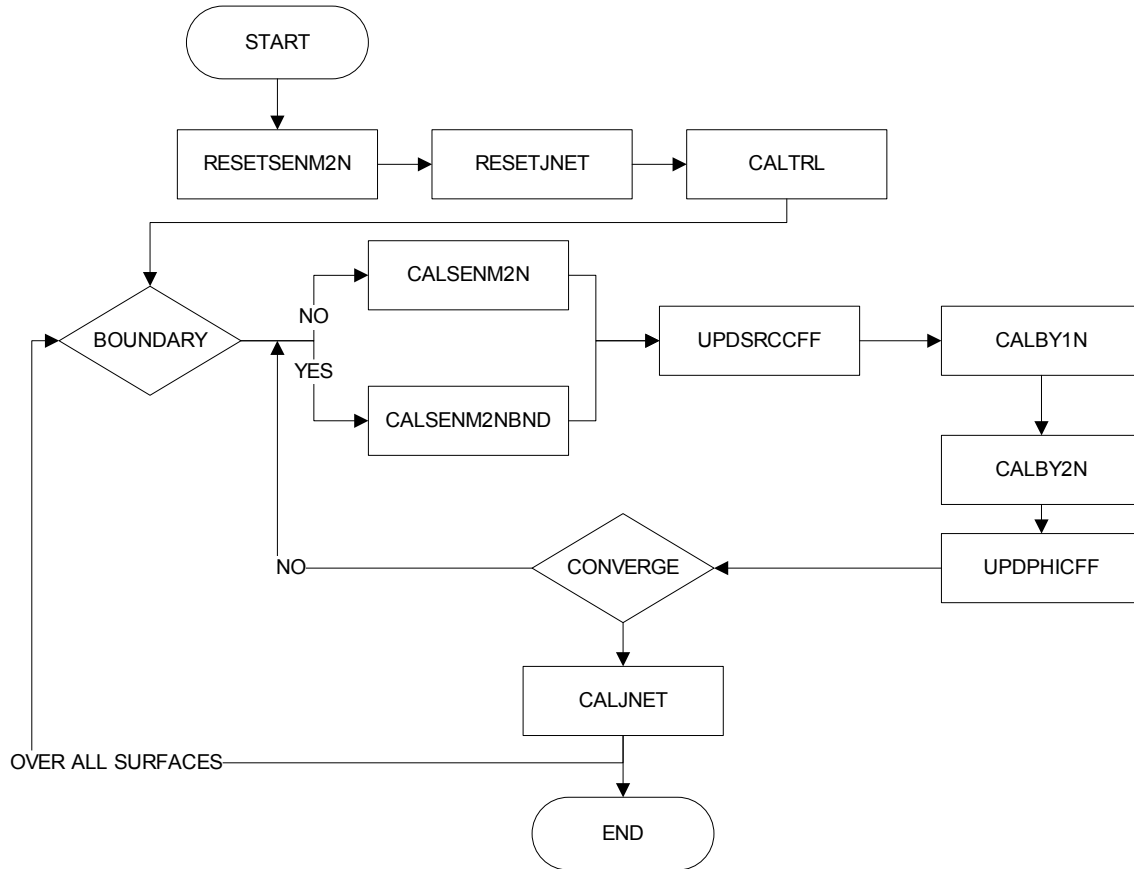


Figure 6 Flow chart of *drivesenm2n*

3.2 Modification of PARCS Code

In PARCS, several subroutines and variables were added or modified to integrate the SENM library.

- **SenmIntgM (added)**
The module *senmintgm* was added to PARCS to integrate the SENM library with PARCS. The module provides several subroutines to initialize and calculate steady-state, transient and pin power reconstruction calculations as an agent for the SENM library which encapsulates the SENM library from PARCS and allows modification of the PARCS code as little as possible.
- **MemAllocM (modified)**
Variables limited to the two-group structure were modified for multi-group calculation and the module *moxtrm* was allocated.
- **InitializedM (modified)**
This was modified to handle the benchmark table-sets and to initialize multi-group fission source terms.

- InpProcM (modified)
In this module, some input variables were added to choose SENM as a solver and solve OECD/NEA MOX Transient benchmark problem with the module *moxtrm*.
- NormalizedM (modified)
The subroutine *norm* of the module *senm* is called when the main solver is configured as the source expansion nodal method.
- XsecFdbkM (modified)
If the input 'FUNC_TYPE' = 20, the option *ioptxsf* is 20 and the *xsecmox* which calculates cross-sections for the MOX transient benchmark problem is called.
- SSeigM (modified)
This was modified to call *outersss* of *senmintgm* when SENM is chosen as the steady-state solver.
- TransDriverM (modified)
The subroutine *outertr* of *senmintgm* was added in the subroutine *transient* of this module.
- DepMainM (modified)
The subroutine *driveppr* of *senmintgm* is called when the solver is set as SENM.
- Parcsexe (modified)
The subroutine *senmintg* of *senmintgm* is called after finishing initialization which is executed with *p_init* in this subroutine when SENM is assigned for 'NODAL_KERN' in the input file.
- ItrcntIM (modified)
The logical variable *lisenm* was added to check whether the solver is SENM or not.

4. VERIFICATION

The OECD/NEA AND U.S. NRC PWR MOX/UO₂ CORE TRANSIENT BENCHMARK Problem [9] published by Purdue University in 2003 was used for verification of the newly implemented multi-group solver. The benchmark problem report contains four parts representing calculation results for steady-states in various conditions and a fast transient as follows:

- Part I: Multiplication factor, rod worth, assembly and pin power at fixed T/H conditions
- Part II: Critical boron concentration, assembly and pin power at HFP
- Part III: Critical boron concentration, assembly and pin power at HZP
- Part IV: Simulation of control rod ejection accident from HZP conditions

Fundamental functionalities of the multi-group routines, such as implementation of numerical formulations and basic integration with PARCS, are evaluated in Part I. And then, the steady-state routines including integration with T/H routines of PARCS are tested and the performance for solving the steady-state problem in various conditions is assessed in Parts II and III. Finally, the transient routines are evaluated in Part IV and computational performance of the new multi-group routines is compared to the existing routines, additionally. Since the heterogeneous solutions calculated by DeCART in the final benchmark report are used as the references in Parts I and III, accuracy of the new multi-group kernel is evaluated by comparing the calculation results quantitatively to those of the existing nodal and pin power routines. On the other hand, it is tried to verify implementation of the new routines by comparing results qualitatively in Parts II and IV since any heterogeneous solution by DeCART was not provided.

4.1 Part I – 2D Calculation at Fixed T/H Conditions

This part was to solve steady-state problem with two-dimensional core configuration with fixed T/H conditions of hot zero power. The basic capabilities of the multi-group nodal and pin power routines are assessed in this part.

Table 1 shows a comparison of multiplication factors and assembly power errors against Part I of the benchmark report. All solutions determined by the SENM kernel match well to the results determined by the ANM and NEM kernels at ARO and ARI conditions. Comparing two-group results indicated by ANM 2G and SENM 2G, it is verified that the source expansion nodal method has an accuracy equivalent to the ANM solution. The multi-group results of the SENM kernel are also comparable to those of the existing NEM kernel.

Like the existing kernels, assembly power distributions of the SENM kernel were in a very good agreement to the heterogeneous solution by the DeCART code at ARI as well as ARO conditions in all group structures within 1 ~ 2% of PWE and EWE. It was noticeable that the two-group results agree well with the reference contrary to the expectation that the assembly power distribution makes a larger distortion in the MOX loaded core. The reason could be found in the spatial discretization. Since the cross-section is not interpolated for the fixed T/H condition, the difference in reaction rates between the homogeneous and heterogeneous solutions is only ascribable to the spatial discretization which is unrelated to the group configuration.

Table 1 Comparison of eigenvalue and assembly power

Nodal Kernel	Eigenvalue		TOTAL ROD WORTH [dk/k, pcm]	Assembly Power Error			
	ARO	ARI		ARO		ARI	
				%PWE	%EWE	%PWE	%EWE
ANM 2G	1.06379	0.99154	6850	0.96	1.63	1.67	2.18
SENM 2G	1.06379	0.99154	6850	0.83	1.63	1.57	2.18
NEM 4G	1.06376	0.99136	6865	0.90	1.42	1.61	2.26
SENM 4G	1.06378	0.99136	6868	0.76	1.47	1.59	2.20
NEM 8G	1.06354	0.99114	6868	0.86	1.25	1.65	2.49
SENM 8G	1.06358	0.99114	6871	0.84	1.29	1.49	2.37
*DeCART	1.05852	0.98743	6801	ref	ref	ref	ref

*DeCART: Reference

Table 2 and Table 3 show the pin power results at the ARO condition. Like the eigenvalue and the assembly power, the pin power results also agree very well with the reference results. The existing pin power kernel of PARCS was based on the corner point balancing method with corner discontinuity and provided accurate results because it solved the two-dimensional neutron diffusion equation analytically, but it was only applicable to the two-group problems. On the other hand, the new source expansion pin power reconstruction kernel provides accurate results with any group structures as shown in the tables. There is slight difference between the two-group and multi-group results but they are consistent with respect to the assembly power distributions.

Table 2 Pin power %PWE at ARO

Nodal Kernel	Assembly Position					
	(A, 1)	(B,2)	(C,3)	(D,4)	(E,5)	(F,6)
ANM 2G	0.28	0.21	0.29	0.54	0.32	0.51
SENM 2G	0.23	0.25	0.33	0.41	0.28	0.77
NEM 4G	-	-	-	-	-	-
SENM 4G	0.23	0.21	0.35	0.36	0.30	0.77
NEM 8G	-	-	-	-	-	-
SENM 8G	0.28	0.18	0.38	0.41	0.32	0.57

Table 3 Pin power %EWE at ARO

Nodal Kernel	Assembly Position					
	(A,1)	(B,2)	(C,3)	(D,4)	(E,5)	(F,6)
ANM 2G	0.54	0.45	0.41	0.79	0.60	1.05
SENM 2G	0.73	0.52	0.60	1.06	0.78	6.63
NEM 4G	-	-	-	-	-	-
SENM 4G	0.75	0.48	0.60	1.03	0.82	6.10
NEM 8G	-	-	-	-	-	-
SENM 8G	0.94	0.50	0.67	1.07	0.84	5.68

4.2 Part II – 3D calculation at Hot Full Power Conditions

Part II describes three-dimensional steady-state calculations with thermal-hydraulic feedback at hot full power condition. Unlike Part I, the PARCS 2G calculation results are used as the basis for comparison of assembly and pin-power distribution, since there exist no reference results calculated by DeCART in the final report of the benchmark problem. Critical boron concentrations, assembly power and core-averaged T/H properties are compared for different nodal kernels and group structures in Table 4.

The critical boron concentrations calculated by the SENM 2G kernel are very close to the ANM 2G results within one ppm and the assembly power distributions and core-averaged T/H properties are essentially identical. The SENM kernel shows good agreement with the existing NEM kernel in four- and eight-group calculation results.

Table 4 Comparison of CBC, assembly power and core average T/H properties

Nodal Kernel	Critical Boron Concent. [ppm]	Ass. Power Error		Core Average T/H Properties				
		%PWE	%EWE	Doppler Temp. [K]	Mod. Density [kg/m3]	Mod. Temp. [K]	Outlet Mod. Density [kg/m3]	Outlet Mod. Temp. [K]
ANM 2G	1679	ref	ref	836.0	706.1	581.3	662.1	598.8
SENM 2G	1678	0.00	0.02	836.2	706.1	581.3	662.1	598.8
NEM 4G	1674	0.31	0.50	836.1	706.1	581.3	662.1	598.8
SENM 4G	1675	0.03	0.34	836.2	706.1	581.3	662.1	598.8
NEM 8G	1672	0.55	0.86	836.2	706.1	581.3	662.1	598.8
SENM 8G	1673	0.39	0.69	836.2	706.1	581.3	662.1	598.8

The SENM kernel appears to determine properly the axial power distributions in Figure 7 but noticeable differences are found near the top and bottom axial reflecting regions as shown in

Figure 8. The axial power distributions of the SENM kernel show about 7 ~ 8 % differences from those of the ANM result near the reflectors, while they are quite similar near the center. This is because the assembly discontinuity factor is considered along the axial direction as well as the radial direction in the SENM kernel but not in the existing kernels. From these results, it can be judged that the source expansion nodal routines have been integrated well with routines for T/H feedbacks and cross-section handling with interpolation in PARCS. The multi-group results are also similar to the two-group results.

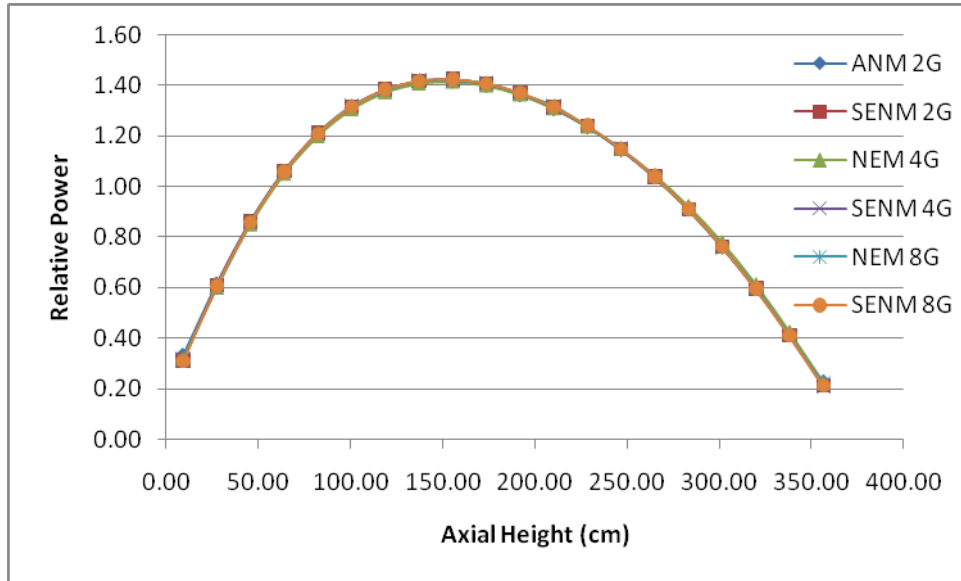


Figure 7 Axial power distribution

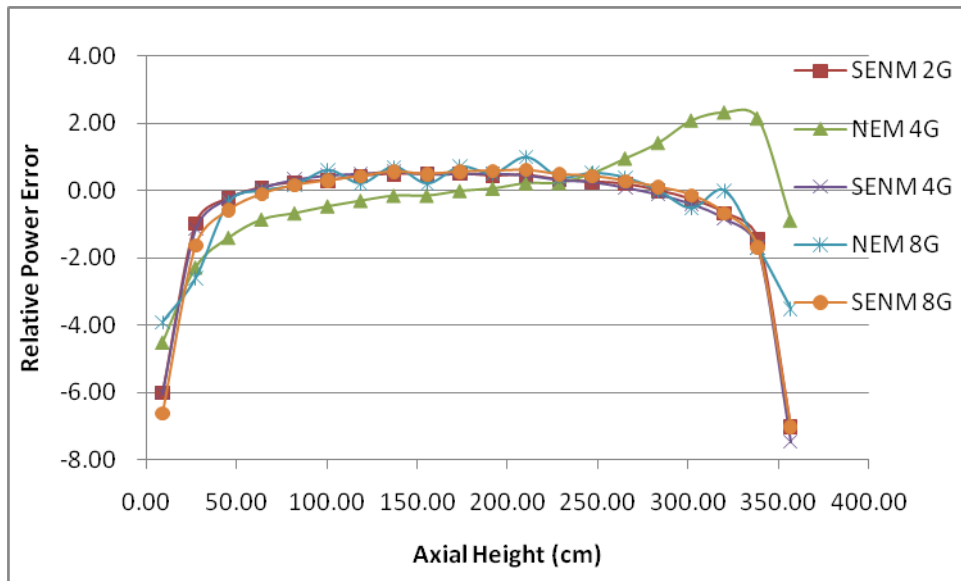


Figure 8 Axial power distribution error

Comparison of pin-power distributions are shown in Table 5 and Table 6. Comparing with the results of the ANM 2G kernel, the SENM kernel gave reasonable results with the two- and multi-group structures.

Table 5 Pin power %PWE at HFP

Nodal Kernel	Assembly Position					
	(A,1)	(B,2)	(C,3)	(D,4)	(E,5)	(F,6)
ANM 2G	ref	ref	ref	ref	ref	ref
SENM 2G	0.00	0.00	0.00	0.00	0.02	0.25
NEM 4G	-	-	-	-	-	-
SENM 4G	0.00	0.00	0.02	0.03	0.14	0.41
NEM 8G	-	-	-	-	-	-
SENM 8G	0.10	0.01	0.03	0.33	0.18	0.39

Table 6 Pin power %EWE at HFP

Nodal Kernel	Assembly Position					
	(A,1)	(B,2)	(C,3)	(D,4)	(E,5)	(F,6)
ANM 2G	ref	ref	ref	ref	ref	ref
SENM 2G	0.35	0.35	0.35	0.35	0.35	5.00
NEM 4G	-	-	-	-	-	-
SENM 4G	0.36	0.35	0.36	0.38	0.40	4.60
NEM 8G	-	-	-	-	-	-
SENM 8G	0.37	0.37	0.36	0.47	0.45	4.05

4.3 Part III – 3D Calculation at Hot Zero Power Conditions

Part III of the benchmark problem report describes the steady-state at hot zero power condition. The critical boron concentration and assembly power distributions results are shown in Table 7. Since the errors due to the cross-section interpolation and feedback handling are negligible at HZP conditions, the error are mainly ascribable to the spatial discretization. The assembly power errors become slightly larger than those of Part I because the effect of spatial discretization increases in three-dimensional calculations. But all of the nodal kernels show good agreements with the reference solution.

Table 7 Comparison of critical boron concentration and assembly power

Nodal Kernel	CBC [ppm]	*Assembly Power Error	
		%PWE	%EWE
ANM 2G	1341	1.05	3.49
SENM 2G	1340	1.04	3.49
NEM 4G	1337	1.11	3.06
SENM 4G	1337	1.09	3.22
NEM 8G	1334	1.20	2.85
SENM 8G	1335	1.14	2.91

*Assembly Power Error: the DeCART result is used as the reference

Axial power distributions and the relative errors at each axial location are shown in Figures 9 and 10, respectively. Since the axial reflector model has a large effect on determining the axial power distribution, the same axial reflector model is used for all cases of calculations in this benchmark problem. The axial power distributions generated by SENM kernel are in a good agreement with the reference results in all axial regions, whereas the existing nodal kernels of PARCS show large relative errors of about 6 ~ 10 % in the top and bottom fuel regions. The reason why the existing nodal kernels show such large errors near the reflector regions seems that the assembly discontinuity factor is not considered in the axial direction. From these results, it can be concluded that the assembly discontinuity factor should be also considered in the axial direction.

Table 8 and Table 9 show the results of pin power calculations. In the three-dimensional pin power calculation, two-dimensional pin power calculation is performed several times for each plane and the radial pin power distribution is obtained by averaging the plane-wise pin powers over the axial direction. The pin power results show similar trends with the results of Part 1 for different nodal kernels and group structures. In this calculation, it was worthwhile to note that the source expansion pin power reconstruction works well for three-dimensional calculations as well as two-dimensional calculations.

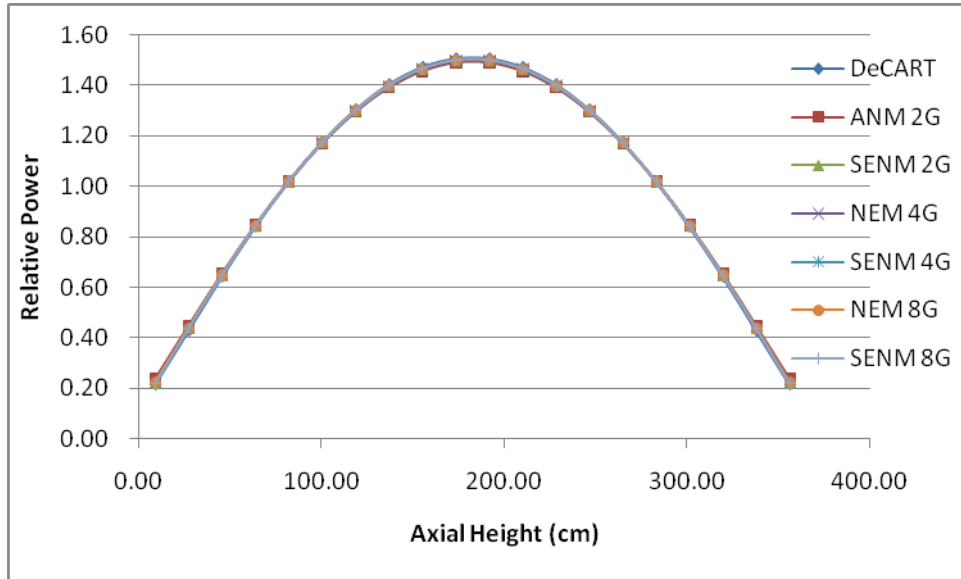


Figure 9 Axial power distribution at HZP conditions

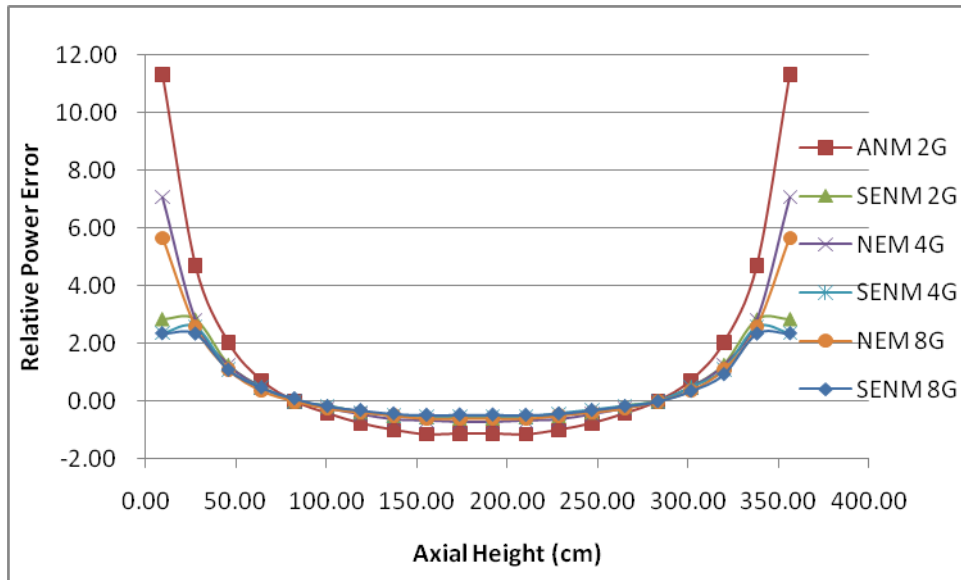


Figure 10 Axial power distribution error at HZP conditions

Table 8 Pin power %PWE at HZP conditions

Nodal Kernel	Assembly Position		
	(B,2)	(D,4)	(F,6)
ANM 2G	0.82	0.62	0.48
SENM 2G	0.78	0.51	0.71
SENM 4G	0.78	0.46	0.72
SENM 8G	0.76	0.44	0.60

Table 9 Pin power %EWE at HZP conditions

Nodal Kernel	Assembly Position		
	(B,2)	(D,4)	(F,6)
ANM 2G	1.83	1.39	0.90
SENM 2G	1.83	1.71	5.76
SENM 4G	1.88	1.85	5.39
SENM 8G	1.85	1.88	5.06

4.4 Part IV – 3D Transient Calculation

In Parts I ~ III, capabilities of the source expansion nodal and pin power kernels have been evaluated and their performance was found superior for steady-state problems. In this section, the transient capability is evaluated by simulating a fast transient accident in which a single rod is ejected in 0.1 second. Like Part II, the transient results are not compared to the reference results, but the results of SENM kernel are compared with those of existing nodal kernels qualitatively because any reference results are not given in Part IV of the benchmark report. The ejected rod worth is about 1.13\$ so that it causes a super-prompt critical transient involving a sharp power pulse from the hot-zero-power condition.

In Table 10, peak time, peak power and power integral are compared and Figure 11 shows transient core power behaviors. From these comparisons, one can conclude that the two-group results calculated by the SENM kernel are essentially identical to the results of the ANM kernel and the SENM kernel provides the same accuracy as the analytic solution in transient calculations as well as steady-state calculations. In case of the multi-group results, the SENM and the NEM kernels show a slight difference of about 10% in the peak power whereas they show coincidence in their peak times. It was found in a previous work regarding the source expansion methodology that the results of NEM kernel approach to those of the SENM kernel as number of nodes per fuel assembly is increased. The SENM kernel simulates one-dimensional flux shape using the trigonometric functions and therefore provides better results than the NEM kernel.

Table 10 Transient peak power and power integral

Nodal Kernel	Peak Time [sec]	Peak Power [%]	Power Integral [%-sec]
ANM 2G	0.34	142	27.2
SENM 2G	0.34	146	27.3
NEM 4G	0.33	152	27.8
SENM 4G	0.33	163	28.4
NEM 8G	0.32	172	29.1
SENM 8G	0.32	180	29.8

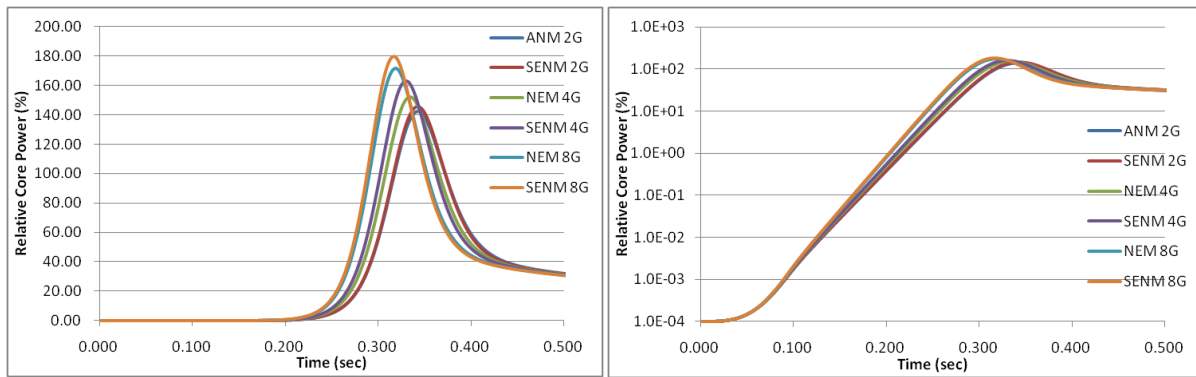


Figure 11 Transient core power behavior

Behaviors of transient assembly peaking and three-dimensional point pin peaking factors are shown in Figure 12 and 13, respectively. While the existing routines were only able to calculate the two-group transient pin power distribution, the new routines are able to calculate it with all group structures as shown in the figures. The assembly and pin peakings increase quickly during the rod ejection period and then decreases slowly with T/H feedback. Especially, the multi-group transient calculation of the source expansion pin power reconstruction routines has been verified by the fact that the pin peaking behavior of the multi-group calculation agrees well with that of the existing two-group calculation.

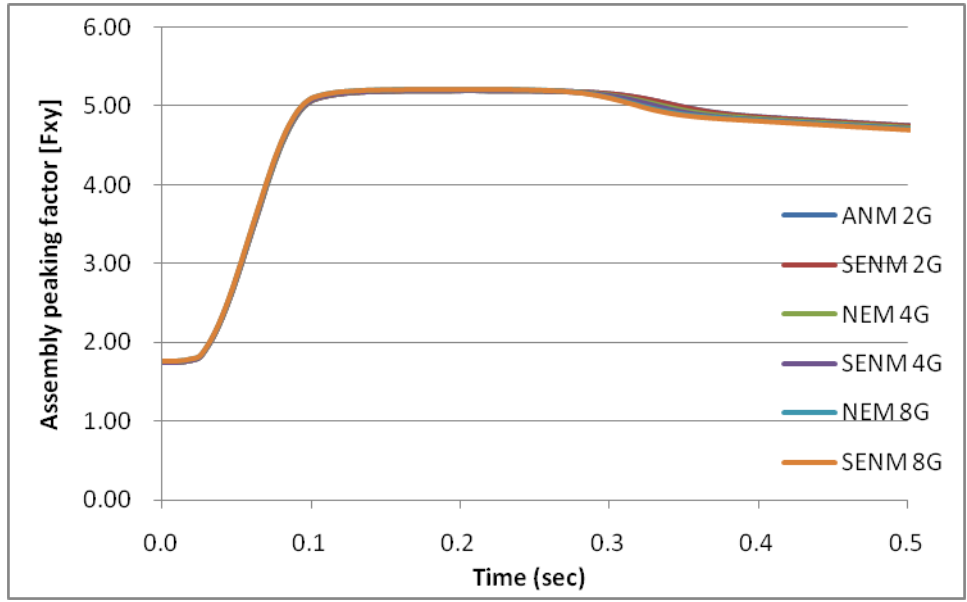


Figure 12 Transient assembly peaking factor

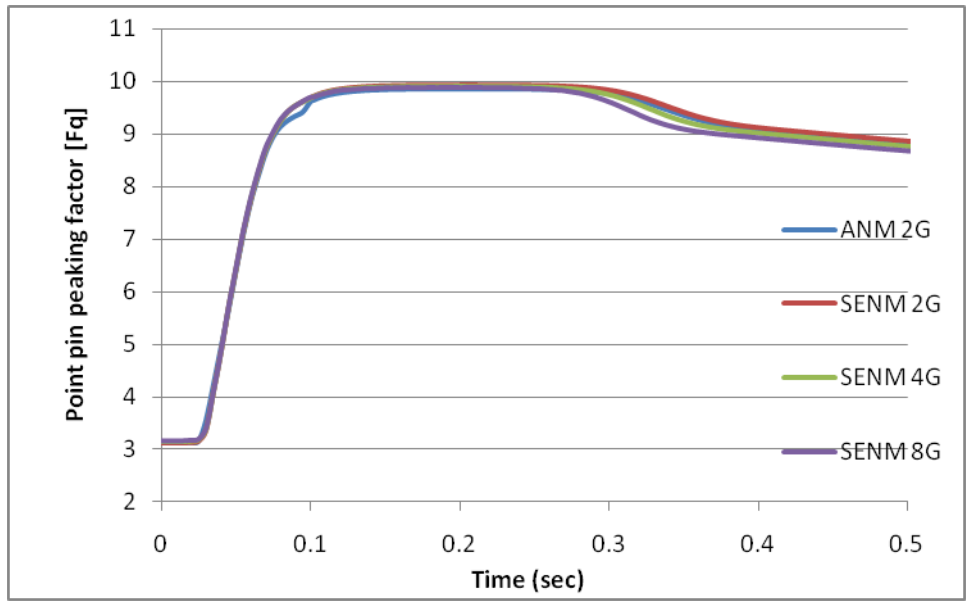


Figure 13 Transient point pin peaking factor

The transient behavior of T/H properties such as the Doppler temperature, the moderator density and moderator temperature are shown in Figure 14, 15 and 16, respectively. Since the same T/H routines are used with similar power behaviors, these are also in good agreements.

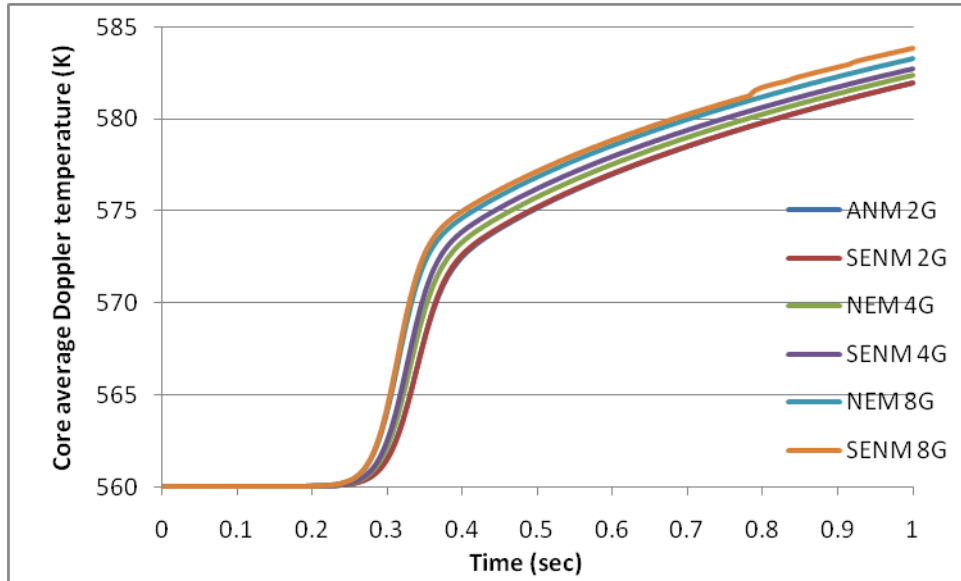


Figure 14 Transient core average Doppler temperature

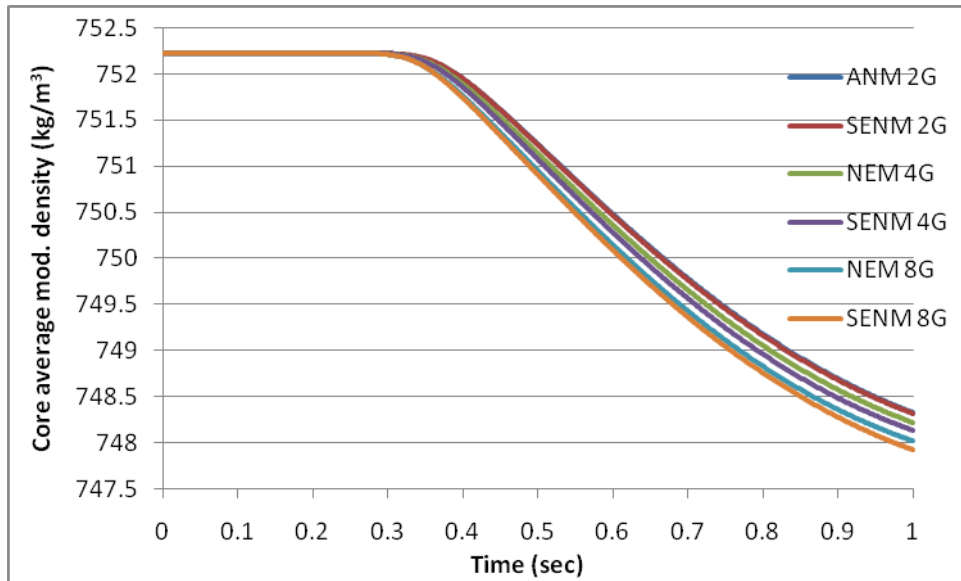


Figure 15 Transient core average moderator density

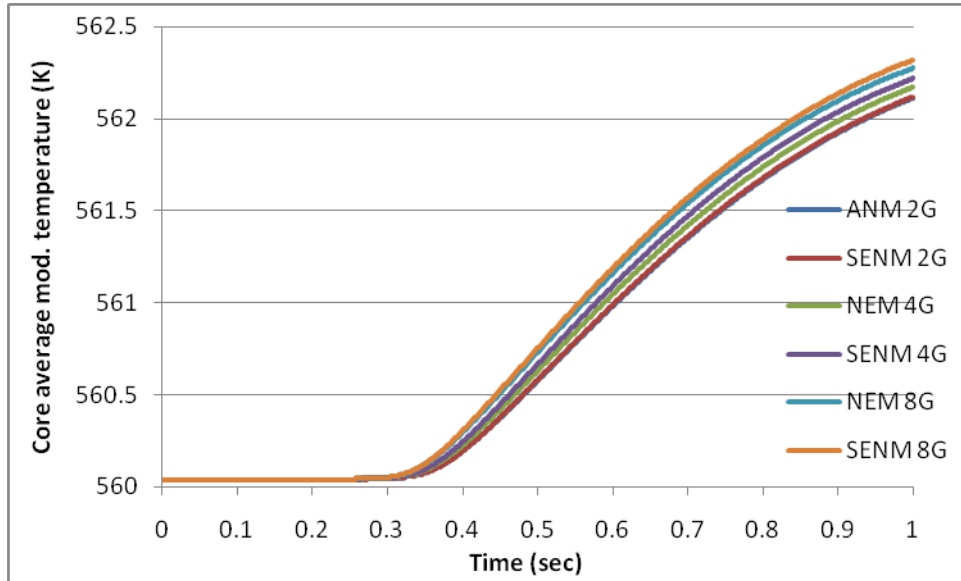


Figure 16 Transient core average moderator temperature

4.5 Computing Time Performance

One of the main reasons to develop efficient multi-group nodal method is to enhance the computational performance of the existing NEM kernel in which one-node nodal expansion method is accelerated by two-group CMFD formulation. The computing times taken for calculations of Parts II and IV are compared to assess the computational performance of the SENM kernel. The computing environment is as follows.

- CPU: Intel Xeon CPU E5520 2.27Ghz X 2
- MEMORY: DDR3 10600 12.0GB
- OPERATING SYSTEM: Windows 7 Professional 64 Bit Edition

Table 11 shows the iteration information of each multi-group nodal kernel. Compared with the existing kernels, the SENM kernel shows much faster computing performance than the NEM kernel. The largest difference in the computing performance is found in the nodal calculation. The NEM kernel takes computing time more than 10 times that of the SENM kernel. Since SENM 8G takes about 1.04 second per iteration which is about two times 0.46 second of SENM 4G, the computing time seems to be proportional to the number of energy groups in case of SENM kernel. However, the computing time of the NEM kernel is proportional to the square of energy groups as 3.15 seconds of NEM 4G is increased to 11.27 seconds for NEM 8G. By these results, the SENM kernel shows a superior computing performance especially for multi-group calculations.

Computing performance of the nodal kernels becomes more important in transient problems because they take much more iterations and time.

Table 12 compares elapsed times taken for Part IV calculations. The calculation time differ by about 5000 seconds in case of the eight-group structured problem which should be a considerable advantage in analyzing reactor core transients.

Table 11 Comparison of computing times for the steady-state calculation (Part II)

Nodal Kernel	NODAL		CMFD		XSEC	MISC.	TOTAL
	Iter. #	Time (sec)	Iter. #	Time (sec)	Time (sec)	Time (sec)	Time (sec)
NEM 4G	15	47.31	44	6.06	3.94	0.22	57.53
SENM 4G	9	4.11	49	3.36	1.59	0.23	9.30
NEM 8G	12	135.29	-	5.01	5.89	0.24	146.44
SENM 8G	8	8.33	47	6.72	4.19	0.19	19.42

Table 12 Comparison of computing time for the transient calculation (Part IV)

Nodal Kernel	NODAL+CMFD	OTHERS	TOTAL
	Time (sec)	Time (sec)	Time (sec)
NEM 4G	1696.6	221.0	1917.6
SENM 4G	473.1	178.4	651.5
NEM 8G	6306.8	390.0	6696.8
SENM 8G	957.4	497.9	1455.3

5. CONCLUSIONS

An efficient multi-group solution based on source expansion nodal method consisting of nodal and pin power calculation schemes has been formulated successfully for multi-group problems. The source expansion formulation is to expand source terms located on the right hand side of the neutron balance equation with a set of polynomial functions and provides the decoupled groupwise neutron balance equations which can be solved more easily than the coupled equations. Source iteration is essentially needed to achieve more exact solutions.

The source expansion nodal scheme solving the transverse-integrated one-dimensional neutron balance equation is coupled with the multi-group CMFD formulation to find the global neutron flux distribution. And the two-level CMFD scheme in which two-group CMFD calculation accelerates the multi-group CMFD calculation is also employed. All of the modules in *cmfd* category provide subroutines and variables for the two-level CMFD calculation and the source expansion nodal method is implemented in the *senm* category. In addition, the BICG preconditioned by incomplete LU factorization is implemented in the *bicg2g* and *bicgmg* categories to solve the CMFD linear systems. The pin power reconstruction with the source expansion approach is implemented into the *ppr* category with consideration of the corner discontinuity factor.

The numerical coding is written in the form of a static library of FORTRAN90 and all subroutines of the library except the *main* category is encapsulated from PARCS. This programming strategy can make the library independent from the PARCS code and allows easy maintenance of routines. Also, it minimizes modification of the PARCS code.

In order to evaluate the newly implemented routines in terms of accuracy and speed, the OECD/NEA AND U.S. NRC PWR MOX/ UO_2 CORE TRANSIENT BENCHMARK Problems was chosen as the reference. Throughout all parts of the benchmark problem containing steady-state and transient cases, the new source expansion kernel provides enhanced accuracy compared to the existing nodal expansion kernel. Especially, the multi-group pin power which is not obtainable with the original kernel has become available with the new source expansion kernel and agrees well with the reference. The source expansion kernel is about 4 times faster than the nodal expansion kernel in the 3D real-size core problems. From the results, it is concluded that the newly implemented source expansion kernel provides a good accuracy, yet very fast calculation speed regardless the structure of energy groups chosen.

6. REFERENCES

1. H. G. Joo, D. A. Barber, G. Jiang and T. J. Downar, "PARCS, A Multi-Dimensional Two Group Reactor Kinetics Code Based on the Nonlinear Analytic Nodal Method," PU/NE-98-26, Sept. 1998.
2. P.D. Esser and K.S. Smith, "A Semi-Analytic Two-Group Nodal Model for SIMULATE-3," *Trans. Am. Nucl. Soc.*, **68**, 220, 1993.
3. V. G. Zimin, H. Ninokata and L. R. Pogobekyan, "Polynomial and Semi-Analytic Nodal Methods for Nonlinear Iteration Procedure," *Proc. Int. Conf. Phys. Nucl. Sci. Tech. (PHSOR-98)*, Long Island, NY, October 5-8, 1998, **2**, 994, 1998.
4. V. G. Zimin and H. Ninokata, "Nodal Neutron Kinetics Model Based on Nonlinear Iteration Procedure for LWR Analysis," *Ann. Nucl. Energy*, **25**, 507, 1998.
5. Y. I. Kim, Y. J. Kim, S. J. Kim and T. K. Kim, "A Semi-Analytic Multigroup Nodal Method," *Ann. Nucl. Energy*, **26**, 699, 1999.
6. X. D. Fu and N. Z. Cho, "Nonlinear Analytic and Semi-Analytic Nodal Methods for Multigroup Neutron Diffusion Calculations," *J. Nucl. Sci. Tech.*, **39**, 1015, 2002.
7. D. J. Lee, T. J. Downar and Y. H. Kim, "Convergence Analysis of the Nonlinear Coarse-Mesh Finite Difference Method for One-Dimensional Fixed-Source Neutron Diffusion Problem," *Nucl. Sci. Eng.*, **147**, 127, 2004.
8. T. Y. Han, H. G. Joo and C. H. Kim, "Two-Group CMFD Accelerated Multi-Group Calculation with a Semi-Analytic Nodal Kernel," *Proc. PHYSOR 2006, ANS Topical Mtg. on Reactor Physics*, Vancouver, B.C., Canada, Sept. 10-14, 2006.
9. T. Kozlowski and T. Downar, "Pressurized Water Reactor MOX/UO₂ Core Transient Benchmark, Final Report," OECD Nuclear Energy Agency, 2006.
10. Böer, R and Finnemann, H., "Fast Analytical Flux Reconstruction Method for Nodal Space-Time Nuclear Reactor Analysis," *Annl. Nucl. Energy*, **19**, 617, 1992.
11. J. I. Yoon and H. G. Joo, "Two-Level Finite Difference Formulation with Multigroup Source Expansion Nodal Kernel," *Journal of Nuc. Sci. and Tech.*, **45**, 668, 2008.

NRC FORM 335 (9-2004) NRCMD 3.7	U.S. NUCLEAR REGULATORY COMMISSION 1. REPORT NUMBER (Assigned by NRC, Add Vol., Supp., Rev., and Addendum Numbers, if any.) NUREG/IA-0416				
BIBLIOGRAPHIC DATA SHEET (See instructions on the reverse)					
2. TITLE AND SUBTITLE Implementation of Advanced Multigroup Nodal and Pin Power Reconstruction Methods into PARCS 3.1	3. DATE REPORT PUBLISHED <table border="1" style="width: 100%;"> <tr> <td style="width: 50%; text-align: center;">MONTH</td> <td style="width: 50%; text-align: center;">YEAR</td> </tr> <tr> <td style="text-align: center;">May</td> <td style="text-align: center;">2012</td> </tr> </table> 4. FIN OR GRANT NUMBER 	MONTH	YEAR	May	2012
MONTH	YEAR				
May	2012				
5. AUTHOR(S) Joo-Il Yoon, Han-GyuJoo, Seung-Hoon Ahn	6. TYPE OF REPORT Technical 7. PERIOD COVERED (Inclusive Dates) 				
8. PERFORMING ORGANIZATION - NAME AND ADDRESS (If NRC, provide Division, Office or Region, U.S. Nuclear Regulatory Commission, and mailing address; if contractor, provide name and mailing address.) <table style="width: 100%;"> <tr> <td style="width: 33%;">KEPCO Nuclear Fuel Daejeon, Korea</td> <td style="width: 33%;">Seoul National University Seoul, Korea</td> <td style="width: 33%;">Korea Institute of Nuclear Safety Daejeon, Korea</td> </tr> </table>		KEPCO Nuclear Fuel Daejeon, Korea	Seoul National University Seoul, Korea	Korea Institute of Nuclear Safety Daejeon, Korea	
KEPCO Nuclear Fuel Daejeon, Korea	Seoul National University Seoul, Korea	Korea Institute of Nuclear Safety Daejeon, Korea			
9. SPONSORING ORGANIZATION - NAME AND ADDRESS (If NRC, type "Same as above"; if contractor, provide NRC Division, Office or Region, U.S. Nuclear Regulatory Commission, and mailing address.) Division of Systems Analysis Office of Nuclear Regulatory Research U.S. Nuclear Regulatory Commission Washington, DC 20555-0001					
10. SUPPLEMENTARY NOTES A. Calvo, NRC Project Manager					
11. ABSTRACT (200 words or less) <p>The original multi-group solver of PARCS uses a nodal expansion method combined with one-node calculation scheme. But the neutronics solver was inefficient for application to the real-size reactor cores because of its slow performance. Moreover, the existing pin power reconstruction with the corner point balancing method does not support the multi-group structure. In order to improve the performance for multi-group problems, the semi-analytic nodal method and pin power reconstruction with the source expansion formulation have been incorporated into the PARCS code. The purpose of the nodal formulation is to solve the transverse-integrated one-dimensional neutron balance equation. Also, a two-level CMFD method in which the two-group CMFD is used for accelerating the multi-group CMFD calculation has been constructed to improve the calculation efficiency. The newly implemented routines are written in the form of a static library of FORTRAN90 that forms link to the PARCS code during compilation. The new numerical method has been evaluated over benchmark problems for steady-state and transient calculations of real-size reactor core. The calculation results show an excellent agreement with the reference results of the benchmark problem. The computing time of the new routines was about 4 times shorter than that of the original routine.</p>					
12. KEY WORDS/DESCRIPTORS (List words or phrases that will assist researchers in locating the report.) PARCS FORTRAN90 CMFD Neutronics solver nodal expansion method one-node calculation scheme Korean Institute of Nuclear Safety (KINS) MARS code	13. AVAILABILITY STATEMENT unlimited 14. SECURITY CLASSIFICATION (This Page) unclassified (This Report) unclassified 15. NUMBER OF PAGES 16. PRICE 				



Federal Recycling Program



**UNITED STATES
NUCLEAR REGULATORY COMMISSION**
WASHINGTON, DC 20555-0001

OFFICIAL BUSINESS

NUREG/IA-0416

**Implementation of Advanced Multigroup Nodal and Pin Power
Reconstruction Methods into PARCS 3.1**

May 2012